Nanocluster Formation and Stabilization Fundamental Studies: Ranking Commonly Employed Anionic Stabilizers via the Development, Then Application, of Five Comparative Criteria

2 **AUTHORS**, INCLUDING:

Saim Özkar
Middle East Technical University

298 PUBLICATIONS **5,170** CITATIONS

SEE PROFILE

Nanocluster Formation and Stabilization Fundamental Studies: Ranking Commonly Employed Anionic Stabilizers via the Development, Then Application, of Five Comparative Criteria

Saim Özkar[†] and Richard G. Finke*

Contribution from Department of Chemistry, Colorado State University, Fort Collins, Colorado 80523

Received December 21, 2001

Abstract: To start, a brief introduction is provided on the importance of transition-metal nanoclusters, on the need to develop and then apply methods to rank the nanocluster formation and then stabilizing abilities of commonly employed anions, solvents, cations, and polymers, and on the somewhat confused literature of nanocluster stabilization. The fundamental importance of surface-adsorbed *anions* in transition-metal nanocluster stabilization is noted, the reason the present studies begin with a study of nanocluster-stabilizing anions. Next, five criteria, as well as the associated experimental methods, are developed to evaluate the efficacy of nanocluster stabilizing agents. The criteria are of fundamental significance in that they allow the separation of stabilizing agent effects on nanocluster formation from those on nanocluster stabilization. The results from applying the five criteria to four commonly employed anions lead to the first "anion series" of relative nanocluster-formation and stabilizing abilities, at least for the Ir(0) nanoclusters examined and by the following five criteria: $[(P_2W_{15}Nb_3O_{61})_2O]^{16-}$ (a Brφnsted-basic polyoxoanion) > $C_6H_5O_7^{3-}$ (citrate trianion) > $[-CH_2-CH(CO_2)-]_n^{n-}$ (polyacrylate) ~ Cl^-. In addition to the needed methods and the first anion series, six other (8 total) conclusions are reached, important insights in an area previously lacking hard information about which anions are the better choices for nanocluster formation and stabilization. The results are also of significance in establishing polyoxoanions, notably highly charged and basic polyoxoanions such as $[(P_2W_{15}Nb_3O_{61})_2O]^{16-}$, as the present "Gold Standards" among currently known nanocluster stabilizing anions, and according to the above five criteria. Such standards provide a reference point for future work aspiring to develop even better nanocluster stabilizing anions, solvents, cations, and polymers or their combinations.

Introduction

Transition-metal nanoclusters are of significant current interest for their unique chemical and physical properties arising from their nanodimensions.[1–4] Nanoscopic materials have many possible applications, including quantum dots[5] or quantum computers,[6] optical, electronic, or magnetic devices,[7] chemical sensors,[8] ferrofluids for cell separations,[9] and components in industrial lithography,[10] as well as in applications in photochemical devices such as flat-panel displays.[11] Chemical catalysis by transition-metal nanoclusters—that is, new types

* Corresponding author. E-mail: rfinke@lamar.colostate.edu.
† On Sabbatical leave from Middle East Technical University, Department of Chemistry, 06531 Ankara, Turkey.

(1) Reviews: (a) Schmid, G.; Baumle, M.; Geerkens, M.; Heim, I.; Osemann, C.; Sawitowski, T. *Chem. Soc. Rev.* **1999**, *28*, 179. (b) Schmid, G.; Chi, L. F. *Adv. Mater*. **1998**, *10*, 515. (c) Fendler, J. H., Ed. *Nanoparticles and Nanostructured Films*; Wiley-VCH: Weinheim, 1998. (d) Fürstner, A., Ed. *Active Metals: Preparation, Characterization, and Applications*; VCH: Weinheim, 1996. (e) Bradley, J. S. In *Clusters and Colloids. From Theory to Applications*; Schmid, G., Ed.; VCH: New York, 1994; pp 459–544. (f) Schmid, G. *Chem. Rev.* **1992**, *92*, 1709. (g) A superb series of papers, complete with a record of the insightful comments by the experts attending the conference, is available in: *Faraday Discuss.* **1991**, *92*, 1–300. (h) Schmid, G. In *Aspects of Homogeneous Catalysis*; Ugo, R., Ed.; Kluwer: Dordrecht, 1990; Chapter 1. (i) Andres, R. P.; Averback, R. S.; Brown, W. L.; Brus, L. E.; Goddard, W. A., III; Kaldor, A.; Louie S. G.; Moscovits, M.; Peercy, P. S.; Riley, S. J.; Siegel, R. W.; Spaepen, F.; Wang, Y. *J. Mater. Res.* **1989**, *4*, 704. (j) Henglein, A. *Chem. Rev.* **1989**, *89*, 1861. (k) Thomas, J. M. *Pure Appl. Chem.* **1988**, *60*, 1517. (l) Jena, P.; Rao B. K.; Khanna, S. N. *Physics and Chemistry of Small Clusters*; Plenum: New York, 1987.

(2) (a) Aiken, J. D., III; Finke, R. G. *J. Mol. Catal. A: Chem.* **1999**, *145*, 1. (b) Aiken J. D., III; Lin, Y.; Finke, R. G. *J. Mol. Catal. A: Chem.* **1996**, *114*, 29. (c) Finke, R. G. Transition-Metal Nanoclusters: Solution-Phase Synthesis, then Characterization and Mechanism of Formation, of Polyoxoanion- and Tetrabutylammonium-Stabilized Nanoclusters. In *Metal Nanoparticles: Synthesis, Characterization and Applications*; Feldheim, D. L., Foss, C. A., Jr., Eds.; Marcel Dekker: New York, 2002; Chapter 2, pp 17–54.

(3) (a) Turton, R. *The Quantum Dot: A Journey into the Future of Microelectronics*; Oxford University Press: New York, 1995. (b) Haberland, H., Ed. *Clusters of Atoms and Molecules*; Springer-Verlag: New York, 1994.

(4) (a) Schmid, G., Ed. *Clusters and Colloids; From Theory to Applications*; VCH Publishers: New York, 1994. (b) de Jongh, L. J., Ed. *Physics and Chemistry of Metal Cluster Compounds*; Kluwer Publishers: Dordrecht, 1994.

(5) Simon, U.; Schön, G.; Schmid, G. *Angew. Chem., Int. Ed. Engl.* **1993**, *32*, 250.

(6) Glanz, J. *Science* **1995**, *269*, 1363.

(7) (a) Schön, G.; Simon, U. *Colloid Polym. Sci.* **1995**, *273*, 202. (b) Antonietti, M.; Göltner, C. *Angew. Chem., Int. Ed. Engl.* **1997**, *36*, 910. (c) Thomas, J. M. *Pure Appl. Chem.* **1988**, *60*, 1517. (d) Colvin, V. L.; Schlamp, M. C.; Alivisatos, A. P. *Nature* **1994**, *370*, 354.

(8) Elghanian, R.; Storhoff, J. J.; Mucic, R. C.; Letsinger, R. L.; Mirkin, C. A. *Science* **1997**, *277*, 1078.

(9) Sonti, S. V.; Bose, A. *J. Colloid Interface Sci.* **1995**, *170*, 575.

(10) Reetz, M. T.; Winter, M.; Dumpich, G.; Lohau, J.; Friedrichowski, S. *J. Am. Chem. Soc.* **1997**, *119*, 4539.

of highly active and selective catalysts—is another currently important driving force behind the rapid development of transition-metal nanoclusters.[12]

The high interest in transition-metal nanoclusters engenders a high interest in how nanoclusters are optimally formed and stabilized. The stabilization of transition-metal nanoclusters is, however, the subject of a confusing literature. For example, a 1995 *Science* paper on Pd(0) nanoclusters[13] claims the implausible[14] direct coordination of a R_4N^+ cation to the nanocluster's electrophilic surface, a point of confusion in other, recent nanocluster work as well.[15,16] The broad picture of the mechanisms of stabilization of transition-metal nanoclusters should not be as confused as it is. Specifically, there is considerable precedent in the colloid literature,[17] and in Derjaguin–Landau–Verway–Overbeek (DLVO) theory of colloidal stability in the 1940s, for the general stabilization mechanisms of colloidal materials.[18] In that literature colloidal stabilization is well established to involve both (i) *charge stabilization* by the surface adsorbed anions such as chloride or citrate^{3-}, Figure 1a,[19] plus (ii) *steric stabilization* by the presence of polymers such as the often used poly(vinylpyrrolidone), Figure 1b.[17,20]
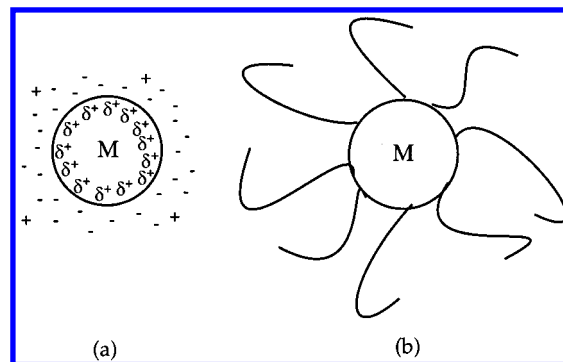

Figure 1. A schematic illustration for (a) an electrostatically stabilized metal (M) particle (i.e., one stabilized by the adsorption of ions and the resultant electrical double layer), adapted from the literature,[17a] and (b) a sterically stabilized metal particle (i.e., one stabilized by the adsorption of polymer chains, for example).[17b]

Note that fundamental to this picture is a layer of surface-adsorbed *anions,* or polymers, which kinetically stabilize the

(11) Vossmeyer, T.; DeIonno, E.; Heath, J. R. *Angew. Chem., Int. Ed. Engl.* **1997**, *36*, 1080.

(12) (a) Stein, J.; Lewis, L. N.; Gao, Y.; Scott, R. A. *J. Am. Chem. Soc.* **1999**, *121*, 3693. (b) Reetz, M. T.; Breinbauer, R.; Wedemann, P.; Binger, P. *Tetrahedron* **1998**, *54*, 1233. (c) Schmidt, T. J.; Noeske, M.; Gasteiger, H. A.; Behm, R. J.; Britz, P.; Brijoux, W.; Bönnemann, H. *Langmuir* **1997**, *13*, 2591. (d) Schmid, G.; Maihack, V.; Lantermann, F.; Peschel, S. *J. Chem. Soc., Dalton Trans.* **1996**, 589. (e) Reetz, M. T.; Lohmer, J. G. *Chem. Soc., Chem. Commun.* **1996**, 1921. (f) Reetz, M. T.; Breinbauer, R.; Wanninger, K. *Tetrahedron Lett.* **1996**, *37*, 4499. (g) Reetz, M. T.; Quaiser, S. A.; Merk, C. *Chem. Ber.* **1996**, *129*, 741. (h) Bönnemann, H.; Braun, G. A. *Angew. Chem., Int. Ed. Engl.* **1996**, *35*, 1992. (i). Wilcoxon, J. P.; Martino, T.; Klavetter, E.; Sylwester, A. P. *Nanophase Mater.* **1994**, 771. (j) Lewis, L. N. *Chem. Rev.* **1993**, *93*, 2693. (k) Vargaftik, M. N.; Zargorodnikov, V. P.; Stolarov, I. P.; Moiseev, I. I.; Kochubey, D. I.; Likholobov, V. A.; Chuvilin, A. L.; Zamaraev, K. I. *J. Mol. Catal.* **1989**, *53*, 315.

(13) (a) Reetz, M. T.; Helbig, W.; Quaiser, S. A.; Stimming, U.; Breuer, N.; Vogel, R. *Science* **1995**, *267*, 367. (b) This often cited paper appears to be in error in its interpretations of the larger d_{STM} vs d_{TEM} distances, ascribing them *solely* to the R_4N^+ and ignoring the Br^- that should be present (by Bönnemann's analyses of identically prepared nanoclusters[13c]). The authors were apparently mislead somewhat by Figures 3 and 4 in another paper.[13c] (c) Of interest is Bönnemann's report that reducing PdX_2 (X = Cl, Br, OAc) with $R_4N^+BR_3H^-$ yields R_4N^+ and X^- stabilized, 18–40 Å Pd(0)$_n$ clusters of undefined exact composition, [Pd(0)$_n$Br$_a$Cl$_b$H$_c$O$_d$(OH)$_e$]$^{x-}$ [R_4N^+]$_x$, although he did demonstrate by analysis ca. 83% Pd and 5–6% Cl or Br: Bönnemann, H.; Brijoux, W.; Brinkmann, R.; Dinjus, E.; Jouβen, T.; Korall, B. *J. Mol. Catal.* **1992**, *74*, 323.

(14) (a) A R_4N^+ cation is not expected to coordinate to an electrophilic surface metal in solution where more basic anions and coordinating solvents are present as competing ligands; indeed, there exists no precedent in the organometallic or heterogeneous catalysis literature for R_4N^+ *being a ligand*—the R_4N^+ cation has no unshared electron pairs available for coordination to an electrophilic surface metal atom. Only the σ bonding pairs are "available" as ligands, and organometallic chemists know that only in the absence of other ligands (such as coordinating solvents or multidentate polyoxoanions) can such σ bonds be ligands. The weak bond or dissociation energies (BDE) of such σ bonds to metals are ca. 8–10 kcal/mol as determined by photoacoustic calorimetry,[14b] far less than the 20–40 kcal/mol BDEs of most other ligands well studied in organometallic chemistry.[14c] (b) Yang, G. K.; Peters, K. S.; Vaida, V. *Chem. Phys. Lett.* **1986**, *125*, 566. (c) Collman, J. P.; Hegedus, L. S.; Norton, J. R.; Finke, R. G. *Principles and Applications of Organotransition Metal Chemistry*; University Science Books: Mill Valley, 1987; p 250.

(15) (a) Surprisingly, and apparently because they have not done crucial experiments such as electrophoresis to demonstrate the charge on their nanoclusters, a recent paper implies that their long-chain R_4N^+ cations are simply adsorbed directly onto putative anionically charged nanoclusters (see Figure 4 on p 363 elsewhere[15b] or Figure 12 in a ref 15c); unfortunately, the charge on a colloid or nanocluster particle is *rarely* demonstrated experimentally, and was not demonstrated in either of the cited papers.[15b,c] Moreover, the elemental analyses provided in the paper show the presence of Cl^-, Br^-, or other anions *in every case*; hence, there is no reason to think that the R_4N^+ are adsorbed directly to the metal surface as written, but rather that the anions present (Cl^-, Br^-, or OAc^-) are adsorbed. (b) Bönnemann, H.; Brinkmann, R.; Neiteler, P. *Appl. Organomet. Chem.* **1994**, *8*, 361. (c) See Figure 12 on p 191 in the otherwise very valuable paper by Toshima and his collaborators.[23]

(16) (a) Ultimately, the confusion on the direct interaction of R_4N^+ with metal surfaces can be traced to a 1988 paper[16b] (and its miscitation by others), a paper that (i) studies poorly compositionally characterized Ag(0) nanoparticles by using surface enhanced Raman spectroscopy (SERS), (ii) underemphasizes (but does cite, however, vide infra) the role of the surface-coordinated Br^- that is present, and (iii) has a confusing Figure 3 therein that shows the apparent, nonsensical[14] direct coordination of R_4N^+ to the Ag(0) surface. But, greatly adding to the confusion is (iv) the miscitation of this 1988 paper by others by implying that it gives precedent for a direct coordination of R_4N^+ to the Ag(0) surface. Although the authors of the SERS paper say that the binding of a cationic surfactant (i.e. Me_3NR^+) to a cationic (Ag^+) surface must require the intermediacy of a counteranion (i.e. Br^-), Figure 3 in that paper shows the hypothetical/postulated coordination of the long-chain R_4N^+ directly to the (Ag^+) surface, something that is unreasonable on Coulombic grounds. A later report is also unclear about the type of interaction between the metal surface and the ligands present (in that case ascorbic acid and poly(L-lysine)[16c]). The problems here stem from the fact that the compositions of the nanocluster systems studied are not known exactly. The authors[16b] are apparently unaware that anions (X = NO_3^- or ClO_4^- from the AgX precursor) are present at the Ag^+ surface. The R_4N^+ then follow the anions by charge balance (and are probably ion-paired), but are not adsorbed directly to the surface without anion assistance to bring them close to the surface. A recent SERS study[16d] of tetramethylammonium adsorbed on silver electrodes demonstrates that halide anions indeed exist between the adsorbed R_4N^+ cations and the Ag^+ cations on the electrode surface. (b) Wiesner, J.; Wokaun, A.; Hoffmann, H. *Prog. Colloid Polym. Sci.* **1988**, *76*, 271. (c) Munro, C. H.; Smith, W. E.; White, P. C. *Analyst* **1995**, *120*, 993. (d) Deng, Z.; Irish, D. E. *J. Phys. Chem.* **1994**, *98*, 11169. (e) The following paper claims, for Co clusters and on the basis of susceptibility data, that "only a weak interaction between (the) stabilizer and cluster surface is present": Becker, J. A.; Schäfer, R.; Festag, J. R.; Wendorf, J. H.; Hensel, F.; Pebler, J.; Quaiser, S. A.; Helbig, W.; Reetz, M. T. *Surf. Rev. Lett.* **1996**, *3*, 1121.

(17) For a general discussion on the stability of colloids or nanoclusters see, for example: (a) Hirtzel, C. S.; Rajagopalan, R. *Colloidal Phenomena: Advanced Topics*; Noyes Publications: Westwood, NJ, 1985; pp 27–39, 73–87. (b) Hunter, R. J. *Foundations of Colloid Science*; Oxford University Press: New York, 1987; Vol .1, pp 316–492.

(18) Evans, D. F.; Wennerström, H. *The Colloidal Domain*, 2nd ed.; Wiley-VCH: New York, 1999.

(19) (a) Note that the positive charge on the metal surface, of at least neutral nanoclusters, is better described as an *electrostatic charge mirror* induced by the adsorption of the anions to the coordinatively unsaturated, electron-deficient, initially neutral metal surface.[19b,c] (b) Labib, M. E. *Colloids Surf.* **1988**, *29*, 293. (c) Brockris, J. O'M.; Reddy, A. K. N. *Modern Electrochemistry*; Plenum Press: New York, 1973; Vol. II.

(20) However, hindering this older, colloidal literature from having a wider, better accepted impact is the central, underlying weakness of much of traditional colloidal science: the *ill-defined compositions* of traditional colloids. Witness, for example, the confusion[13,14] caused, ultimately, by studies of the poorly compositionally characterized nanoclusters "[(Ag(0))$_a$(Ag(surface)$^+$$_b$(X$^-$)$_c$(EDTA)$_d$]$^{b-c}$[Me$_3NR^+$]$_{b-c}$" (X$^-$ = an ill-defined, apparent mixture of Br^- and NO_3^- or ClO_4^- or deprotonated EDTA) and by the misleading Figure 3 elsewhere[16b] showing a putative direct coordination of Me_3NR^+ to the Ag(0) nanocluster surface. This lack of precise knowledge of the composition of traditional colloids rules out rigorous comparisons and conclusions concerning the true sources, and their relative significance, of the stabilization mechanisms of nanoscopic metal particles. Precise compositional knowledge is of course a well-known, primary tenant of rigorous chemical science. There is no reason to abandon the rigors of smaller molecule science in achieving the goals of what has been termed nano-*molecular* science[2c] to distinguish it from the less rigorous nanomaterials science.

colloids electrostatically, or sterically, respectively, thereby slowing the rate of particle agglomeration.[21] The resultant, often anionic particles electrostatically repel each other, thereby providing the particles with Coulombic ("charge repulsion") kinetic stabilization toward agglomeration. The countercations necessary for charge balance, plus more anions, are typically present in what is closely analogous to the electrical double-layer at an electrode surface,[19b] Figure 1a. The fundamental position of surface-adsorbed anions in nanocluster stabilization is why the present investigations *begin with a study of different anions* (and not solvents, cations, or polymers).

At present, there is no way to choose rationally which anionic stabilizers, solvents, countercations, or polymer additives are truly optimum to maximize the formation, stabilization, and then desired physical property of a given transition-metal nanocluster. The two prior methods to rate colloidal stabilizing agents are more than 35 and 100 years old, respectively; moreover, they are not applicable to modern, nonaqueous nanoclusters.[22] A recent collaborative effort among five nanocluster research groups echos the problem in judging the efficacy of a given nanocluster synthesis, noting that, in general, it is not possible to "understand which (nanocluster) preparation method (i.e., with its accompanying different anions, solvents, cations, and polymer stabilizers) is the best among those proposed".[23] A series of relative "nanocluster-stabilizing abilities" would be enormously helpful in guiding future work about which anions and other components are best. In the case of anionic stabilizers, present work in the field often uses rather different anions such as citrate^{3-} ($C_6H_5O_7{}^{3-}$), polyacrylate^{n-} ($[-CH_2-CH(CO_2{}^-)-]_n{}^{n-}$), Cl$^-$, or polyoxoanions^{n-} (such as $[(P_2W_{15}Nb_3O_{61})_2O]^{16-}$) without any true insights into which anion is really preferred or why.[24] Identification of the "Gold Standards" among stabilizing anions, solvents, cations, and polymers would also be very valuable so that the field would then have a focal point for comparative studies of new stabilizers seeking to provide even greater nanocluster stabilization.

Foremost among the needed investigations, then, is the development of the actual modern methods and criteria by which to study and compare various stabilizers. Reflection reveals, however, that even more basic studies are required before the

methods underlying the desired nanocluster formation and stabilization comparative studies can be performed. Specifically, there is a need for a prototype transition-metal nanocluster system in which the following prior studies and resultant features are available, features needed to compare different nanocluster stabilizers: (a) a well-defined nanocluster formation reaction with an unequivocally established stoichiometry and a reaction that can be used with a range of other anions, solvents, cations and polymers;[25,26] (b) a nanocluster formation reaction that leads to compositionally well-defined nanoclusters, ideally nanoclusters that are as well characterized as any in the extant literature and where water, oxygen, and other such complicating factors are absent;[2,25,26] (c) a nanocluster system where it is also known that a neutral nanocluster core is formed (e.g., from the balanced reaction stoichiometry), and where the rarely measured charge on the resultant nanoclusters has also been unequivocally established (e.g., by electrophoresis and other methods), so that there is *experimental confirmation* that the anions, for example, are coordinating to the nanocluster surface (and, hence, that the charge mechanism of nanocluster electrostatic kinetic stabilization is operative);[27] *(d) a nanocluster system where the difficult problem of how to monitor the kinetics of nanocluster growth has been overcome and is generally applicable;[28]* and (e) a nanocluster system where detailed, quantitative insights into the nanocluster mechanism of formation are available.[28] In addition, further requirements of the ideal system are as follows: (f) a nanocluster system in which the key experimental criteria are in hand (e.g., nanocluster isolability;[25,26] redissolvability;[25,26] TEM observations;[25,26] catalytic activity;[26,29] and total catalytic lifetime[29]); and, again in the ideal case, (g) a nanocluster system in which the stabilizing anion is as close as possible at the start

(21) Examples of charge or polymer stabilized colloids in *aqueous solution* are the following: (a) Yeung, S. A.; Hobson, R.; Biggs, S.; Grieser, F. *J. Chem. Soc., Chem. Commun.* **1993**, 378. (b) Nagata, Y.; Watananabe, Y.; Fujita, S.-I.; Dohmaru, T.; Taniguchi, S. *J. Chem. Soc., Chem. Commun.* **1992**, 1620. (c) Schmid, G.; Lehnert, A. *Angew. Chem., Int. Ed. Engl.* **1989**, *28*, 780. (d) Van Rheenen, P. R.; McKelvy, M. J.; Glaunsinger, W. S. *J. Solid State Chem.* **1987**, *67*, 151. (e) Harriman, A.; Thomas, J. M. *Nouv. J. Chim.* **1987**, *11*, 757. (f) Nakao, Y.; Kaeriyama, K. *J. Colloid Interface Sci.* **1986**, *110*, 82. (g) Natanson, G.; Amar, F.; Berry, R. S. *J. Chem. Phys.* **1983**, *78*, 399. (h) Boutonnet, M.; Kizling, J.; Stenius, P.; Maire, G. *Colloids Surf.* **1982**, *5*, 209−25. (i) Faraday, M. *Philos. Trans. R. Soc.* **1857**, *147*, 145.

(22) (a) Historically, the "gold number" [22b] or "protective value" [22c] was used as a rough estimate of the ability of a given agent to stabilize an aqueous gold colloid against aggregation or flocculation[43] by a NaCl solution. Note that both these classical tests are only for Au colloids, and then only in aqueous solution. (b) The "gold number" is defined as the weight in mgs of the protecting agent that is just insufficient to prevent 10 mL of a red sol from changing to violet upon the addition of 1 mL of a 10% aqueous NaCl solution: Zsigmondy, R. Z. *Anal. Chem.* **1901**, *40*, 697. (c) The "protective value" is defined as the number of grams of a red sol that is just protected against (visual) flocculation by 1% NaCl by 1 g of the protective agent for ∼3 min: Thiele, H.; Van Levern, H. S. *J. Colloid Sci.* **1965**, *20*, 679. Even this more recent test suffers from problems with the compositionally ill-defined,[20] somewhat irreproducibile, large (ca. 250 Å), aqueous Au colloids it employs—materials rather different than compositionally well-defined, reproducible, smaller, and organic-solvent soluble modern nanoclusters.[2]

(23) Toshima, N.; Shiraishi, Y.; Terannishi, T.; Miyake, M.; Tominaga, T.; Watanabe, H.; Brijoux, W.; Bönneman, H.; Schmid, G. *Appl. Organomet. Chem.* **2001**, *15*, 178.

(24) (a) Pd nanoclusters have been reported to be faster cyclohexene hydrogenation catalysts when the anions are Br$^-$ > Cl$^-$ > OAc$^-$ > I$^-$: Bönnemann, H.; Brinkmann, R.; Neiteler, P. *Appl. Organomet. Chem.* **1994**, *8*, 361. (b) Blum and Vollhardt also report that Br$^-$ > Cl$^-$ (i.e., for the RhX$_4{}^-$ precursor): Badrieh, Y.; Blum, J.; Amer, I.; Vollhardt, K. P. C. *J. Mol. Catal.* **1991**, *66*, 295. Blum, J.; Bitan, G.; Marx, S.; Vollhardt, K. P. C. *J. Mol. Catal.* **1991**, *66*, 313. Azran, J.; Buchman, O.; Amer, I.; Blum, J. *J. Mol. Catal.* **1986**, *34*, 229. (c) The RhX$_4{}^-$ precursor leads to Rh(0) nanocluster catalysts: Weddle, K. S.; Aiken, J. D., III; Finke, R. G. *J. Am. Chem. Soc.* **1998**, *120*, 5653. (d) Halides are well-known to influence soluble Pd(0)$_n$ made from MX$_n$ (X = halide) precursors, for example, Catalytica's "greener" Wacker process, Grate, J. H.; Hamm, D. R.; Mahajan, S. In *Polyoxometalates: From Platonic Solids to Anti-Retroviral Activity*; Pope, M. T., Müller, A., Eds.; Kluwer Academic Publishers: Dordrecht, The Netherlands, 1994; pp 281−305, see pp 295−298. (e) For the established role of Cl$^-$ in the stability of the epoxidation of ethylene by O$_2$ with Ag$_n$ catalysts see: Van Santen, R. A.; Kuipers, H. P. C. E. *Adv. Catal.* **1987**, *35, 265*. Roberts, J. T.; Madix, R. J. *J. Am. Chem. Soc.* **1988**, *110*, 8540. Sajowski, D. J.; Boudart, M. *Catal. Rev. Sci. Eng.* **1987**, *29*, 325.

(25) Lin, Y.; Finke, R. G. *J. Am. Chem. Soc.* **1994**, *116*, 8335.

(26) Lin, Y.; Finke, R. G. *Inorg. Chem.* **1994**, *33*, 4891.

(27) Such a charge-stabilization picture is demonstrated experimentally by our published work, using electrophoresis and ion-exchange resins,[25,26] showing that Ir$_{∼300}$·{[(P$_2$W$_{15}$Nb$_3$O$_{61}$)$_2$O]$^{16-}$}$_{∼33}$ nanoclusters are indeed anionic due to the polyoxoanions adsorbed (bonded) to their surface. Such demonstrations of a nanocluster's surface charge are rare; they are even rarer where the nanocluster's M(0)$_n$ core is also proven to be uncharged, so that one can conclude unequivocally that the overall anionic charge of the nanocluster must be due to the (polyoxo) anion's coordination to the M(0) nanocluster's surface.

(28) For an introduction to the mechanisms of transition-metal nanocluster formation, including a comprehensive listing of the prior literature in the area, see: (a) Watzky, M. A.; Finke, R. G. *J. Am. Chem. Soc.* **1997**, *119*, 10382 and references therein. (b) Watzky, M. A.; Finke, R. G.; *Chem. Mater.* **1997**, *9*, 3083. (c) Aiken, J. D., III; Finke, R. G. *J. Am. Chem. Soc.* **1998**, *120*, 9545 and references therein to diffusive agglomeration of nanoparticles. (d) Widegren, J. A.; Aiken, J. D., III; Özkar, S.; Finke, R. G. *Chem. Mater.* **2001**, *13*, 312 and references therein.

(29) (a) A total turnover value (TTOs) of 18 000 was reported for the polyoxoanion and tetrabutylammonium cation-stabilized Ir(0) nanoparticles in the original publication.[26] However, a later study improved the value to 36 000 for the same material.[29b] (b) The absolute record is for polyoxoanion and tetrabutylammonium cation-stabilized Rh(0) nanoparticles, 190 000 TTOs: Aiken, J. D., III; Finke, R. G. *J. Am. Chem. Soc.* **1999**, *121*, 8803.

to the current "Gold Standard"[30] stabilizer (so that a rigorous comparison is obtained of the best nanocluster stabilizing anions in present use). There is presently only one such system that matches all of these requirements, the $P_2W_{15}Nb_3O_{62}{}^{9-}$/[($P_2W_{15}$-$Nb_3O_{61})_2O]^{16-}$ polyoxoanion- and Bu_4N^+-stabilized Ir(0) nanocluster system. The reader is referred to a series of papers,[25,26,28,29,31] as well as two reviews,[2] for the experimental evidence supporting this fact.

Herein we report (i) the development of a series of five experimental tests and protocols for testing the nanocluster stabilizing ability of a range of different anions; (ii) a comparison of four common anions or polyanions for their nanocluster stabilizing abilities; and (iii) the first relative series of "anion nanocluster-stabilizing abilities", for at least Ir(0) nanoclusters, of [($P_2W_{15}Nb_3O_{61})_2O]^{16-} > C_6H_5O_7{}^{3-} > [-CH_2-CH-$ $(CO_2^-)-]_n{}^{n-} \sim Cl^-$. The results also (iv) allow a total of eight important conclusions to be drawn, conclusions summarized in the Summary and Conclusions section of the paper.

Elsewhere we use the criteria and comparative methods developed herein (a) to test additional anions beyond those the present space allows[32] and to look at the addition of other bases beyond OH^- (i.e., for scavenging the H^+ produced in nanocluster formation reactions involving H_2 as the reductant, eq 1, vide infra), (b) to formulate a previously unavailable molecular-level model and hypothesis for how the best nanoclusters stabilizing agents are working,[33] a model that provides testable predictions as to what anions will best stabilize other transition-metal(0) nanoclusters, and (c) to pick and then to study the previously overlooked $HPO_4{}^{2-}$ anion,[34] a simple and readily available anion that we have predicted[33,34] may be a good, but previously overlooked, anionic stabilizer for transition-metal nanoclusters. We are also (d) systematically evaluating solvents, cations, and polymers by the criteria and methods developed herein, as well as their preferred combinations, to understand how to best form and stabilize transition-metal nanoclusters.[35]

It is hoped that the present studies, plus our additional work in progress,[33,34] will go far toward establishing a more rigorous base of knowledge and hypotheses from which to develop rationally designed, custom-made stabilizers for transition-metal nanoclusters.

Results and Discussion

Choice of Anions To Be Investigated. Based on the literature,[1–12] the anions chosen for this initial study, as their tetrabutylammonium salts, $[Bu_4N]_qY$, are the following: chloride, (Cl^-),[36] the citrate trianion $(C_6H_5O_7{}^{3-})$,[37–39] polyacrylate $(\{[-CH_2-CH(COO^-)-]_n\}^{n-})$,[40] and the highly charged, C_{3v} symmetry, Wells–Dawson type polyoxoanion, $P_2W_{15}Nb_3$-$O_{62}{}^{9-}$.[41] Note that the actual stabilizer in each case, at least in the absence of added OH^-, is the conjugate acid of Y^-, that is, H^+Y^-, since 1 equiv of $H^+BF_4^-$ is produced in the reaction, eq 1, so that all stabilizers, Y^-, more basic than BF_4^- will be protonated. For this reason, adding 1 equiv of OH^- to uncover any effects of scavenging the 1 equiv of H^+ formed, eq 1, is a simple yet novel part of the present contribution. (See also Bradley's important paper[42] on the effects of the 6 equiv of H^+Cl^- formed from the reaction of H_2PtCl_6 plus H_2 to make Pt/H^+Cl^-/PVP-protected colloids.) Note also that for the mono-protonated conjugate acid of the $P_2W_{15}Nb_3O_{62}{}^{9-}$ polyoxoanion, a subsequent dehydration, Nb–O–Nb bridged anhydride forming reaction occurs, $2[HP_2W_{15}Nb_3O_{62}]^{8-} \rightarrow H_2O + [(P_2W_{15}Nb_3$-$O_{61})_2O]^{16-}$, a point unequivocally demonstrated previously[25,26] and also reconfirmed experimentally herein (vide infra). One can immediately see here an added function of poly-Brønsted-basic stabilizers such as citrate, polyacrylate, or polyoxoanions: they can scavenge the H^+ formed in the common nanocluster formation reaction of H_2 reduction of metal salts, for example, eq 1.

$$1.0\ [Bu_4N]_qY + 1.0\ [(1,5\text{-}COD)Ir(CH_3CN)_2]BF_4 + 2.5\ H_2 \tag{1}$$
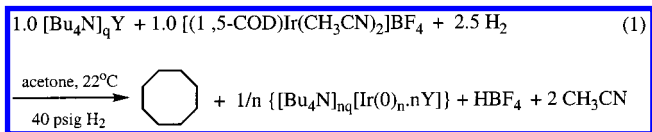
Development of Five Criteria To Measure the Relative Anion Efficiencies for Ir(0) Nanocluster Formation, Stabilization, Catalytic Activity, and Lifetime. The methodologies chosen and developed further herein are derived from our published work.[2,25,26,28] The generalized, balanced equation by which the Ir(0) nanoclusters are prepared is shown in eq 1; experimental evidence for the complete stoichiometry in eq 1

(30) (a) The stabilization provided by Brønsted-basic polyoxoanions is of a little precedented type, one *apparently* due to the *combined high charge* plus *significant steric bulk* present *intrinsically* within the highly negatively charged (9−) and large (ca. 12 × 15 Å) *poly(oxo)anion* and bulky *poly*Bu_4N^+ cation components of $(Bu_4N^+)_9(P_2W_{15}Nb_3O_{62}{}^{9-})$ or its Nb–O–Nb bridged anhydride, $[(P_2W_{15}Nb_3O_{61})_2O]^{16-}$. (b) The large polyoxo-anion size, combined with a specific nanocluster binding site consisting of 3 basic, chelating oxygens, *plus* the lack of anionic charge density in the rest of the polyoxoanion, are a range of features that are not easily matched in other systems. The lack of anionic surface charge density in the rest of the polyoxoanion, that is, past the formally 3 minus "$Nb_3O_9{}^{3-}$" component, can be seen by rewriting the parent polyoxoanion as it actually exists structurally, i.e., $P_2W_{15}Nb_3O_{62}{}^{9-} = \{[(PO_4{}^{3-})_2(W_{15}O_{45})^0(Nb_3O_9)^{3-}]\}^{9-}$—note the *formal* lack of surface anionic charge density on the $(W_{15}O_{45})^0$ part of the polyoxoanion. (High charge density and high ionic strength within the colloid-stabilizing mulitlayer *reduces* its thickness, which in turn gives rise to *less* stable particles, at least in classical H_2O-soluble colloids.[30d] (c) Although the thickness of the multilayer necessarily increases with higher charge polyoxoanions and their associated larger number of accompanying R_4N^+ countercations, a competing *inverse* dependence upon the *charge* (at least in classical H_2O soluble colloids) is the case.[30d] (d) Shaw, D. J. *Introduction to Colloid and Surface Chemistry*, 4th ed.; Butterworth-Heinemann: Boston, 1992; pp 174−176.
(31) Aiken, J. D., III; Finke, R. G. *Chem. Mater.* **1999**, *11*, 1035.
(32) Özkar, S.; Finke, R. G. Submitted for publication (Nanocluster Formation and Stabilization Fundamental Studies. Part II. Proton Sponge as an Effective H^+ Scavenger and Expansion of the Anion Stabilization Ability Series).
(33) Özkar, S.; Finke, R. G. Transition-Metal Nanocluster Stabilization Fundamental Studies: Evidence for High Stabilization by Tridentate Oxoanions and for an Anion-to-Nanocluster Surface Lattice Size-Matching Component. Submitted for publication.
(34) Özkar, S.; Finke, R. G. Transition-Metal Nanocluster Fundamental Studies: Hydrogenphosphate as a Simple, Effective and Readily Available Stabilizer for Well-Formed, Isolable and Redissolvable Ir(0) and Other Transition-Metal Nanoclusters. Submitted for publication.
(35) Hornstein, B. J.; Özkar, S.; Finke, R. G. Unpublished results and experiments in progress.

(36) Schmid, G.; Harms, M.; Malm, J. O.; Bovin, J. O.; van Ruitenbeck, J.; Zandbergen, H. W.; Fu, W. T. *J. Am. Chem. Soc.* **1993**, *115*, 2046.
(37) (a) Enüstün, V.; Turkevich, J. *J. Am. Chem. Soc.* **1963**, *85*, 3317. (b) Turkevich, J.; Kim. G. *Science* **1970**, *169*, 873.
(38) Early use of citrate to stabilize colloids: (a) Turkevich, J. *J. Chem. Phys.* **1945**, *13*, 235. (b) Turkevich, J.; Stevenson, P. C.; Hillier, J. *Discuss. Faraday Soc.* **1951**, *11*, 55. Turkevich, J.; Kim G. *Science* **1970**, *169*, 873. (c) Brugger, P.-A.; Cuendet, P.; Grätzel M. *J. Am. Chem. Soc.* **1981**, *103*, 2923. (d) See also refs 3a−c elsewhere.[25]
(39) (a) Henglein, A.; Giersig, M. *J. Phys. Chem.* **1999**, *103*, 9533. (b) Kamat, P. V.; Flumiani, M.; Hartland, G. V. *J. Phys. Chem.* **1998**, *102*, 3123. (c) Lee, P. C.; Meisel, D. *J. Phys. Chem.* **1982**, *86*, 3391.
(40) (a) Ahmadi, T. S.; Wang, Z. L.; Green, T. C.; Henglein, A.; El-Sayed M. A. *Science* **1996**, *272*, 1924. (b) Ahmadi, T. S.; Wang, Z. L.; Henglein, A.; El-Sayed M. A. *Chem. Mater.* **1996**, *8*, 1161.
(41) (a) Weiner, H.; Aiken J. D., III; Finke, R. G. *Inorg. Chem.* **1996**, *35*, 7905. (b) The $P_2W_{15}O_{56}{}^{12-}$ for the synthesis of the $P_2W_{15}Nb_3O_{62}{}^{9-}$ used herein was all prepared by the improved procedure described in: Hornstein, B. J.; Finke, R. G. *Inorganic Chemistry*. In press (The Lacunary Polyoxoanion Synthon α-$P_2W_{15}O_{56}{}^{12-}$: An Investigation of the Key Variables in Its Synthesis Plus Multiple Control Reactions Leading to a Reliable Synthesis).
(42) Köhler, J. U.; Bradley, J. S. *Catal. Lett.* **1997**, *45*, 203.

is available elsewhere for the well-studied case of the $P_2W_{15}Nb_3O_{62}{}^{9-}$ and $[(P_2W_{15}Nb_3O_{61})_2O]^{16-}$ polyoxoanion-stabilized nanoclusters.[25,26] Note that not all of the 1 equiv of $(Bu_4N)_qY$ (Y = a general anion or polyanion) per 1.0 Ir(I) in the starting complex is coordinated to the resultant nanocluster's metal surface, the rest is part of the stabilizing diffuse layer.[2,25,26]

The five criteria by which the anions are evaluated (with appropriate referencing to earlier, relevant work) are the abilities of a given anion, under identical or otherwise directly comparable conditions, (i) to allow a high level of kinetic control in the formation of the nanoclusters, as measured quantitatively by the k_2/k_1 ratio for the nucleation [A → B (rate constant k_1)], then autocatalytic surface growth [A + B → 2B (the kinetic definition of autocatalysis; rate constant k_2)] mechanism of formation of transition-metal nanoparticles under H_2,[28] where A is the precatalyst complex $[Bu_4N]_5Na_3[(1,5\text{-}COD)Ir\cdot P_2W_{15}Nb_3O_{62}]$, **1**, and B is the catalytically active Ir(0) on the nanocluster's surface. As the present results will show, the larger this ratio (for the cases studied herein), the greater the separation of nanocluster nucleation and growth in time, hence, the closer the resulting nanoparticles become to being monodisperse. The present work will also show that deviations at long reaction times from a good curve-fit, to the nucleation then autocatalytic surface-growth mechanism, are indicative of nanoparticle diffusive agglomeration and, therefore, a lower level of nanoparticle stabilization under the stated reaction conditions. A section in the Supporting Information examines in more detail the conditions required for the correct use of the k_2/k_1 ratio (vs its more rigorous $k_2[B]/k_1$ ratio); that section also examines the limiting values of large and small k_2/k_1 ratios (i.e., see the section A Closer Look at the Proper Use of the k_2/k_1 Ratio and Its Two Interesting Limits, Large vs Small k_2/k_1 Ratios). An important, *empirical* finding from the k_2/k_1 ratio and TEM data presented herein is that the k_2/k_1 ratio[28b] works as expected with larger k_2/k_1 ratios, corresponding to greater separation of nucleation and growth in time, generally corresponding to a narrower size distribution of nanoclusters by TEM.

The remaining criteria are the ability of a given anion (ii) to allow the formation of a narrow, near-monodisperse size dispersion of nanoclusters (i.e., by definition[2] a ≤15% dispersion as judged by TEM imaging of at least a few hundred nanoparticles, so as to provide good statistics on the resultant size distribution), (iii) to allow the nanoclusters to be isolable and, ideally, totally redissolvable without the formation of visible bulk metal—that is, nanoclusters which have sufficient stabilization to allow their isolation by precipitation or evaporation to dryness[43] [this is a fairly rigorous test of nanocluster stabilization in comparison to classic nano*colloids* which generally are not isolable and, therefore, had to be remade each time they were needed (often with catalytic irreproducibility of ±≥500%)],[44] (iv) to permit a high level of catalytic activity, and also (v) to permit a long catalytic lifetime, as measured by the maximum number of total turnovers (TTOs) for the prototype test reaction of cyclohexene olefin hydrogenation, in comparison to the long

catalytic lifetime in solution for $P_2W_{15}Nb_3O_{62}{}^{9-}/[(P_2W_{15}Nb_3O_{61})_2O]^{16-}$ polyoxoanion-stabilized nanoclusters.[29,45]

Note that criteria (i) and (ii) report primarily on *nanocluster formation* while criteria (iii) and (v) probe primarily the anion's ability *to stabilize the nanoclusters*—the first experimental separation of these two, fundamental aspects of optimal nanocluster stabilization. Criteria (iv) and (v) probe the compromise between tight, agglomeration-hindering binding of the anion to the nanocluster's surface vs the availability of open surface sites, the latter being required for catalytic activity. Together, criteria (i)−(v) reflect the need to first *obtain* narrow size distributions of nanoclusters with the desired properties, to then be able to store them in a bottle for future use, and to then have them also possess the desired physical properties, in our case, good catalytic activity and lifetime.

Data for $[(P_2W_{15}Nb_3O_{61})_2O]^{16-}$ and Tetrabutylammonium-Stabilized Iridium(0) Nanoclusters Beginning with the Preformed Precursor, $[Bu_4N]_5Na_3[(1,5\text{-}COD)Ir\cdot P_2W_{15}Nb_3O_{62}]$. It is important to begin with the preformed complex $[Bu_4N]_5Na_3[(1,5\text{-}COD)Ir\cdot P_2W_{15}Nb_3O_{62}]$ (**1**),[46] since we have previously shown this highly reproducible complex yields ±15% reproducible formation kinetics and catalytic activity.[25,26,28] Then, in the next section it will be crucial to demonstrate whether the in situ mixture of $[Bu_4N]_9[P_2W_{15}Nb_3O_{62}]$ and $[(1,5\text{-}COD)Ir(CH_3CN)_2]BF_4$ according to eq 1 yields the same results for the five criteria within experimental error—if so, it allows us to examine all the other anions by the easier, in situ formation route, eq 1.

Hence, to start near-monodisperse $Ir(0)_n$ nanoclusters were prepared as before under what hereafter are called Standard Conditions,[26] that is, the hydrogen reduction of *preformed* 1.2 mM **1** in acetone at 22 °C and in the presence of 1.6 M cyclohexene (serving as a hydrogenation catalysis substrate and, importantly, also as a pseudoelementary step reporter reaction[28] that allows the measurement of k_1 and k_2[28]). A control experiment was done with ultracentrifugation to show that the polyoxoanion produced from the precatalyst **1** and in the *absence* of added OH^- or other base is, as previously found,[25] primarily in its Nb−O−Nb bridged anhydride form, $[(P_2W_{15}Nb_3O_{61})_2O]^{16-}$. The details of this experiment plus the results are available respectively in the Experimental Section and via the Supporting Information (Figure S-1, bottom half).

Figure 2 shows a typical cyclohexene loss vs time curve (the small squares in Figure 2). Experimentally, the H_2 uptake is what is actually measured with use of a high-precision, ±0.01

(43) Classical colloids possess a critical coagulation concentration (ccc), that is, a point in a stability vs added electrolyte curve beyond which they are no longer stable and agglomerate.[18] Interestingly, the most stable nanoclusters made herein (and which contain excess electrolyte beyond that which can be adsorbed on their surfaces; see footnote 43 in ref 25) can be concentrated to dryness as part of their isolation, then redissolved. That is, the most stable nanoclusters prepared herein *lack a ccc* (at least with respect to their own electrolyte), a rather remarkable feature compared to their generally less stable, classical colloid counterparts.

(44) (a) Five-fold (i.e., 500%) rate variations are seen for the photoreduction of CO_2 catalyzed by a series of 10 different batches of the Pd colloids: Willner, I.; Mandler, D. *J. Am. Chem. Soc.* **1989**, *111*, 1330. (b) The difference between nanoclusters and the historically better known nanocolloids is convincingly illustrated by Bradley's seminal paper showing that irreproducibility in the colloid's *composition* of surface-bound Cl^-/H^+Cl^-, the latter being the byproduct of the nanocluster formation reaction, is the origin of the up to 670% irreproducibility in the rate of catalysis by $Pt/PVP/H^+$-Cl^- nanocolloids.[42]

(45) One caveat on the lifetime measurements, a caveat also noted in Table 1: when the presence of a bulk metal precipitate is noted, the TTOs given in Table 1 is an *upper limit* to the TTOs due to nanoclusters alone and as indicated by placing the TTO number in brackets, [TTOs]. See also Table 1, p 4900, in ref 26 for data showing that any bulk metal present generally has a considerably lower surface area in comparison to that of the nanoclusters and, therefore, a significantly slower rate of hydrogenation than the nanoclusters—a fortunate situation that helps limit the contribution of bulk metal to the observed TTO number.

(46) (a) Pohl, M.; Lyon, D. K.; Mizuno, N.; Nomiya, K.; Finke, R. G. *Inorg. Chem.* **1995**, *34*, 1413. (b) Nomiya, K.; Mizuno, N.; Lyon, D. K.; Finke, R. G. *Inorg. Synth.* **1997**, *31*, 186−201. (c) Trovarelli, A.; Finke, R. G. *Inorg. Chem.* **1993**, *32*, 6034. (d) Pohl, M.; Lin, Y.; Weakley, T. J. R.; Nomiya, K.; Kaneko, M.; Finke, R. G. *Inorg. Chem.* **1995**, *34*, 767.
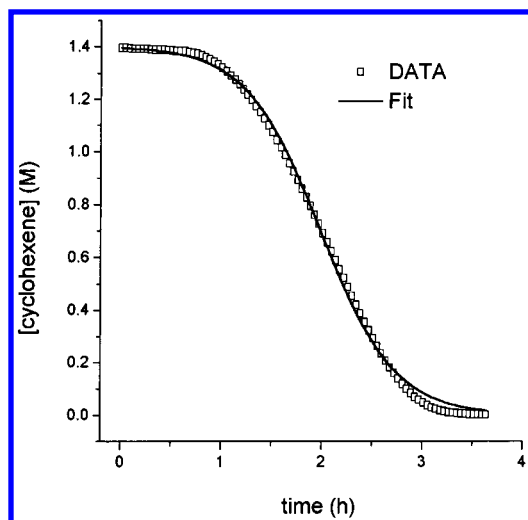
Figure 2. Cyclohexene loss vs time data and curve-fit for the hydrogenation of 1.6 M cyclohexene and concomitant formation of near-monodisperse 22 ± 3 Å Ir(0)$_{\sim 300}$ nanoclusters starting with 1.2 mM [Bu$_4$N]$_5$Na$_3$[(1,5-COD)Ir·P$_2$W$_{15}$Nb$_3$O$_{62}$] in acetone at 22 °C. A 1.0(2) h induction period is seen before the cyclohexene hydrogenation proceeds. The H$_2$ loss (uptake) data are what is actually collected, the pressure rise in the initial part of the curve (due to the solvent vapor pressure reequilibration after 15 flushes with H$_2$ before the reaction was started) is corrected for as described elsewhere[28d] (and, hence, is not seen in this or subsequent figures with kinetic data). The data are then transformed into the cyclohexene loss data in units of M/s as required for the curve-fitting procedure (see the Experimental Section). Note that $-d[H_2]/dt = -d[\text{cyclohexene}]/dt$ due to the 1:1 stoichiometric relationship between H$_2$ and cyclohexene.[28a] From that data the rate, $-d[H_2]/dt = -d[\text{cyclohexene}]/dt = 2.6(2)$ mmol H$_2$/h, listed in Table 1 was calculated from the maximum slope past the induction period. In both this figure and all later cyclohexene loss figures (including those in the Supporting Information), the rate constants for the slow, continuous nucleation, k_1, and autocatalytic surface-growth, k_2, listed in Table 1 were obtained from the nonlinear least-squares curve-fit to the analytic equations[28a] for these two pseudoelementary steps[28a] plus the pseudoelementary hydrogenation reporter reaction,[28a] eqs 2a−c, described in detail elsewhere.[28a] The k_2 value has been corrected by the mathematically required 1400 stoichiometry factor,[28a] both here and in all the other k_2 entries in Table 1 and in the Supporting Information.

psig pressure transducer as detailed in the Experimental Section; note, however, that the H$_2$ uptake and cycloxehexene loss are related by their 1:1 stoichiometry as detailed elsewhere,[28a] so that $-d[\text{cyclohexene}]/dt = -d[H_2]/dt$ can, and will, be used interchangeably as needed.

The sigmoidal shape of the curve in Figure 2 is indicative of the nucleation, then autocatalytic surface-growth, mechanism first elucidated elsewhere.[28] Figure 2 also shows the good curve fit to the analytic equations for the above, two-pseudoelementary-step mechanism[28] plus the hydrogenation catalysis steps (the solid line in Figure 2). The nonlinear least-squares curve fit was accomplished as before and using eqs 2a−c given elsewhere;[28] the resultant rate constants are $k_1 = 0.015(1)$ h^{-1} and $k_2 = 2.8(1) \times 10^3$ M^{-1} h^{-1}. Simple visual analysis of the curve in Figure 2 is also useful since one can readily obtain the induction period, 1.0(2) h, and the slope of the reasonably linear part, $-d[\text{cyclohexene}]/dt = -d[H_2]/dt = 2.6(2)$ mmol H$_2$/h. Elsewhere we have shown that the induction period and $-d[H_2]/dt$ are linearly related to $1/k_1$ and k_2, respectively[28]—that is, it is useful to realize that a long induction period, followed by a sharp downturn to a steep slope, such as seen in Figure 2, *is immediately recognizable as a case with a large k_2/k_1 ratio*. For this reason the induction period and $-d[H_2]/dt$ are also included in Table 1 along with k_1, k_2, and the other data for

criteria (i)−(v) that will be discussed in a moment for the nanocluster precursor (**1**, Table 1, entry 1).

Criterion (ii) is the size and especially the size distribution of the resultant nanoclusters; this was obtained by TEM and is shown in Figure 3 and tabulated in Table 1 (entry 1, column labeled d_m (Å)). For nanoclusters isolated after 14 h and once 1.0 equiv of cyclooctane was evolved as proven by gas−liquid chromatography (1.0 equiv of cyclooctane being required for *complete* nanocluster formation according to eq 1),[26] near-monodisperse (i.e., by definition $\leq \pm 15\%$ at 1σ standard deviation[2]), 22 ± 3 Å Ir(0) nanoclusters are observed, Figure 3a. This general result has been repeated more than 50 times by six independent researchers in our lab. The counting of 405 nontouching particles in Figure 3a was done with the software package NIH Image,[47] a method that minimizes human involvement (but does not eliminate it completely; see the Experimental Section) and, overall, maximizes the number of nanoclusters that can be counted, thereby increasing the quality of the resultant size-distribution statistical data, Figure 3a.

Figure 3b shows an important control reaction: if the nanoclusters are harvested too early (in this case deliberately after 4 h in Figure 3b vs the 14 h for the sample in Figure 3a; that is, after only 60% reduction of the Ir(I) precursor, **1**, to Ir(0) as judged by the 60% evolution of cyclooctane after 4 h), then the resultant size is (as expected) smaller, 15 ± 3 Å, and misleading vs the size of the true, fully formed, 22 ± 3 Å nanoclusters. (The TEM in Figure 3b also *appears* to show more tailing, with its implied diffusive agglomeration,[48] vs the fully formed nanoclusters; however, the inability to visualize nanoclusters below 10 Å means that the distribution is very likely more symmetrical than it appears—that is, caution is needed in such interpretations.) A key point here, then, is the illustration of the very valuable cyclooctane evolution handle for monitoring the formation of the nanoclusters according to eq 1. Without this handle, one might be easily misled about when the nanocluster formation reaction is complete. One might then introduce artifacts by measuring the properties of what is, actually, a mixture of underformed nanoclusters plus their precursor or by measuring artifacts due to agglomeration from nanoclusters that have had to sit long beyond their initial formation. The use of such a monitoring reaction for transition-metal nanocluster formation is, however, and unfortunately, all too rare an occurrence in the extant literature.

Criterion (iii) rates the ability to redissolve the nanoclusters without the formation of visible bulk metal, while criterion (iv) rates the catalytic activity of the *redissolved* nanoclusters, a measurement that tests for both agglomeration (with its associated reduction of the surface area of the nanoclusters) as well as any alternative, surface-poisoning side reactions not prevented by the anion or cations present. As summarized in Table 1 (entry

(47) (a) A separate paper[47b] is under construction on the use of NIH Image[47b] to count nanocluster particles. A recent paper describes the use of a commercial package to count nanoparticles;[47c] unfortunately no comparison exits at present of these two, currently available methods for nanoparticle counting. However, both are rather clearly better than "with a ruler and by-eye" counting, and it seems likely that the packages are otherwise comparable in their features, save the fact that NIH Image is a public domain software. (b) Özkar, S.; Hutchison, J. E.; Finke, R. G. Automatic Counting of Nanoparticles in Transmission Electron Micrograph Pictures Using A Public Domain Image Processing and Analysis Program. To be submitted for publication in *J. Phys. Chem. B.* (c) Reetz, M. T.; Maase, M.; Schilling, T.; Teche, B. *J. Phys. Chem. B* **2000**, *104*, 8779.
(48) Granqqvist, C. G.; Buhrman, R. A. *J. Catal.* **1976**, *42*, 477; see Figure 1 and the discussion about coalescence growth therein.
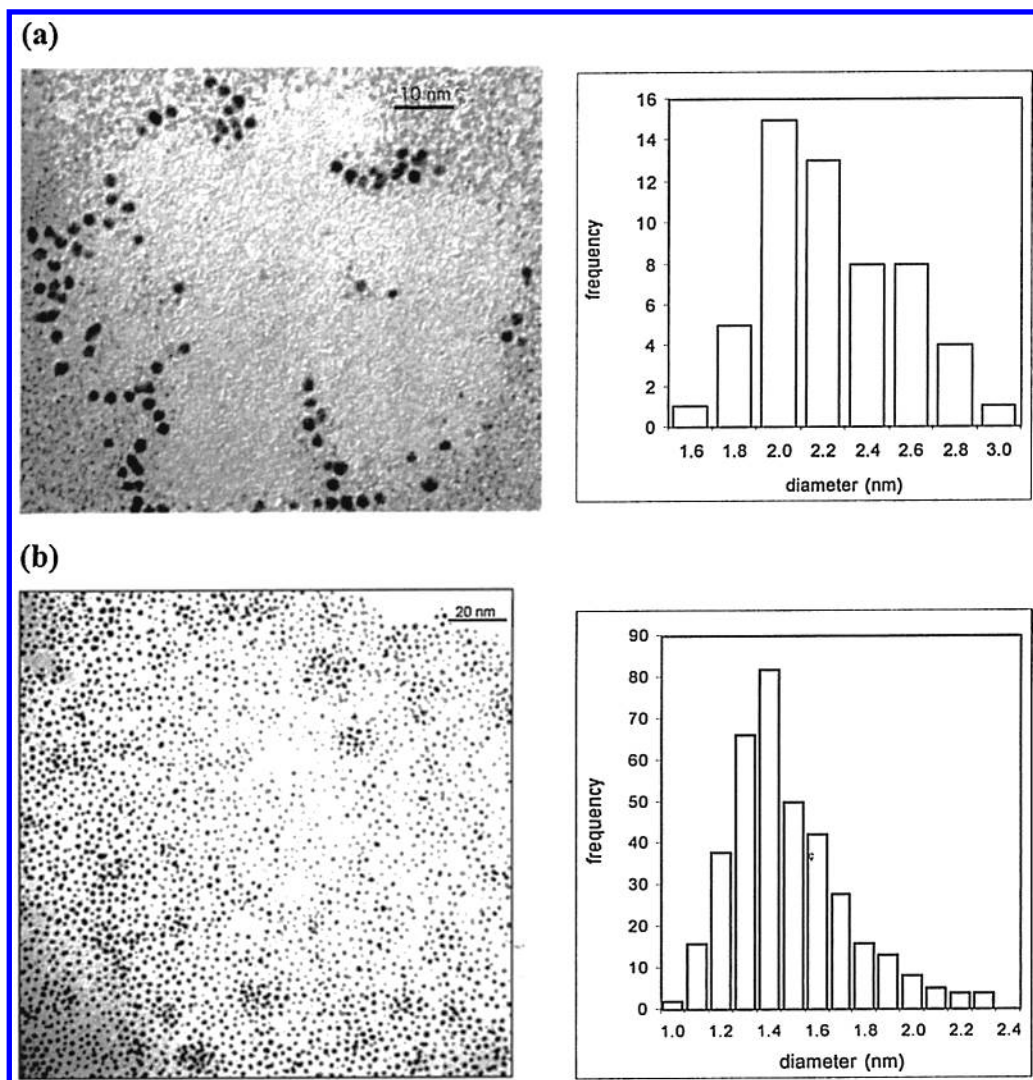
Figure 3. (a) TEM image (580 K magnification) and associated particle size histogram (54 nontouching particles counted by NIH Image as detailed in the Experimental Section) of isolated, near monodisperse[1b] 22 ± 3 Å Ir(0) nanoclusters grown by hydrogen reduction of 1.2 mM [Bu$_4$N]$_5$Na$_3$[(1,5-COD)Ir·P$_2$W$_{15}$Nb$_3$O$_{62}$] in acetone under Standard Conditions. The sample was harvested after 14 h hydrogenation and, therefore, after the nanoclusters are fully formed. (b) TEM image (430 K magnification) and associated particle size histogram (405 nontouching particles counted by NIH Image) of isolated 15 ± 3 Å Ir(0) nanoclusters harvested after only 4 h hydrogen reduction of the same solution (corresponding to about 60% conversion of iridium(I) complex to Ir(0) as determined by GLC monitoring of the cyclooctane evolved during the reduction).

1, columns 9 and 10), the [(P$_2$W$_{15}$Nb$_3$O$_{61}$)$_2$O]$^{16-}$ polyoxoanion-stabilized nanoclusters can be isolated, bottled, and then redissolved in polar organic solvent such as acetone; in addition, they show good cyclohexene hydrogenation catalytic activity once redissolved, 1.9(2) mmol H$_2$/h under Standard Conditions (Table 1, entry 1, column 10). Note also here that it is important not to confuse k_2 with the entries under the cyclohexene hydrogenation "Catalytic Activity" in Table 1: the k_2 value is for a different reduction reaction,[28] namely the ability of the forming nanoclusters to autocatalytically hydrogenate another "A" (i.e., another (1,5-COD)Ir$^+$ as present in **1**).

Criterion (v) rates the ability of each anion to support a large number of TTOs of cyclohexene hydrogenation *in solution*. In the case of the [(P$_2$W$_{15}$Nb$_3$O$_{61}$)$_2$O]$^{16-}$ polyoxoanion-stabilized Ir(0) nanoclusters, 40 000 TTOs over 5 days are observed before deactivation,[29] Figure 4 and Table 1 (entry 1, column 11), a value consistent within ±10% experimental error of the 36 000 TTOs we measured previously.[29b] A bit of perspective is important here: this is a record TTOs lifetime for Ir(0) nanoclusters, but a value lower than the record of 190 000

TTOs for [(P$_2$W$_{15}$Nb$_3$O$_{61}$)$_2$O]$^{16-}$ polyoxoanion-stabilized *Rh(0)* nanoclusters.[29b] Most common-anion stabilized nanoclusters survive but ≤50 TTOs of catalysis *in solution* (see the details and references on p 8804 in ref 29b). G. Schmid first commented on the unusual ability of our polyoxoanions to both stabilize nanoclusters yet allow sufficient nanocluster surface area to be available to allow good catalytic activity, saying that[49] "a special situation has been described where clusters in solution worked as catalysts without recognizable decomposition" (i.e., until their TTOs have ceased). Even then we know that there is no TEM-observable agglomeration, that is, surface deactivation must be the source of the eventual loss of catalytic activity of the polyoxoanion-stabilized nanoclusters.[2,29b]

The Control of in Situ Generation of the Nanocluster Precursors with [(1,5-COD)Ir(CH$_3$CN)$_2$]$^+$BF$_4^-$ Plus [Bu$_4$N]$_9$-[P$_2$W$_{15}$Nb$_3$O$_{62}$]. As noted at the start of the last section, it is important to show that the in situ mixing of [Bu$_4$N]$_9$[P$_2$W$_{15}$-

(49) Schmid, G. In *Applied Homogeneous Catalysis with Organometallic Compounds*; Cornils, B., Herrmann, W. A., Eds.; VCH: New York, 1996; p 641.

Table 1. Compilation of Data for the Four Anionic Stabilizers

entry[a]	precursor	t_{ind} (h)	$(-d[H_2]/dt)$ (mmol H$_2$/h)	k_1 (h^{-1})	$k_2 \times 10^{-3}$ (M^{-1} h^{-1})[b]	$k_2/k_1 \times 10^{-5}$ (M^{-1})[b]	d_m (Å)	appearance	redispersability?	catalytic activity (mmol H$_2$/h)	TTO
[P$_2$W$_{15}$Nb$_3$O$_{62}$]$^{9-}$											
1	[Bu$_4$N]$_5$Na$_3$[(COD)Ir·P$_2$W$_{15}$Nb$_3$O$_{62}$]	1.0(2)	2.6(2)	0.015(1)	2.8(1)	1.9(1)	22(3)	clear, blue^c	yes	1.9(2)	40 000
2	[(COD)Ir(CH$_3$CN)$_2$]BF$_4$ + [Bu$_4$N]$_9$[P$_2$W$_{15}$Nb$_3$O$_{62}$]	1.5(3)	1.7(2)	0.008(1)	1.5(1)	1.9(2)	21(4)	clear, blue^c	yes	0.8(1)	51 000
3	[Bu$_4$N]$_5$Na$_3$[(COD)Ir·P$_2$W$_{15}$Nb$_3$O$_{62}$] + 1 equiv Bu$_4$NOH	0.5(1)	9.0(5)	0.012(1)	6.0(1)	5.0(4)	23(5)	blue,^{c} black particles	partial	2.7(3)	10 000
4	[(COD)Ir(CH$_3$CN)$_2$]BF$_4$ + [Bu$_4$N]$_9$[P$_2$W$_{15}$Nb$_3$O$_{62}$] + equiv Bu$_4$NOH	1.0(2)	1.6(2)	0.008(1)	3.2(1)	4.0(5)^d		blue,^{c} black particles	partial	0.3(1)	
[C$_6$H$_5$O$_7$]$^{3-}$											
5	[(COD)Ir(CH$_3$CN)$_2$]BF$_4$ + [Bu$_4$N]$_3$C$_6$H$_5$O$_7$	2.0(2)	1.8(2)	0.022(2)	1.1(1)	0.50(5)	23(5)	brown, black particles	partial	0.4(1)	[43 000]^e
6	[(COD)Ir(CH$_3$CN)$_2$]BF$_4$ + [Bu$_4$N]$_3$C$_6$H$_5$O$_7$ + 1 equiv Bu$_4$NOH	0.2(1)	2.3(2)	Diff.	Mech.		22(5)	clear, brown	yes	0.5(1)	12 000
Polyacrylate											
7	[(COD)Ir(CH$_3$CN)$_2$]BF$_4$ + 1 equiv poly(acrylic acid, [Bu$_4$N] salt)	0.1(1)	10(1)	0.60(5)	6.3(1)	0.11(1)		clear, black particles	no		
8	[(COD)Ir(CH$_3$CN)$_2$]BF$_4$ + 5 equiv poly(acrylic acid, [Bu$_4$N] salt)	0.1(1)	10(1)	1.1(1)	3.5(1)	0.032(3)		brown, black particles	partial	10(2)	
Cl$^-$											
9	[(COD)Ir·Cl]$_2$	0.1(1)	12(1)	0.030(5)	11(1)	3.6(7)		clear, black particles	no		
10	[(COD)Ir·Cl]$_2$ + Bu$_4$NOH	0.2(1)	26(2)	0.30(1)	14(1)	0.47(4)		clear, black particles	no		

^{a} Entry 1 is the average of seven experiments, entry 2 is the average of three experiments, while all the other entries are the average of two experiments, except when bulk metal was seen (i.e., and the resulting experiment was, therefore, of less interest). ^{b} The k_2 values are corrected by the mathematically required stoichiometry factor of 1400 as detailed elsewhere.[28a] ^{c} The blue color is due to the well-established formation of a two-electron reduced heteropolyblue due to reduction of two W(VI) in the polyoxoanion to two W(V). ^{d} The rate constants k_1 and k_2 are estimates obtained from the curve-fit of the ca. first half of the data only (due to the observation of agglomeration in the ca. second half of the reaction). ^{e} Due to the formation of bulk metal, the values in [ ] brackets are upper limits to the true nanoparticle TTOs.[45]
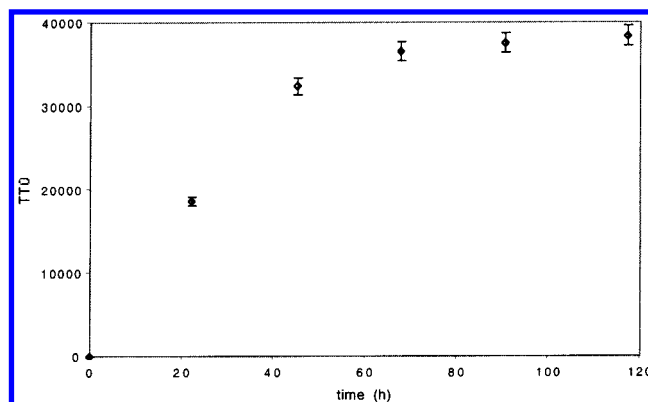

Figure 4. Plot of the total turnovers (TTOs) as a function of time for the hydrogenation of cyclohexene by 8×10^{-5} M [Bu$_4$N]$_5$Na$_3$[(1,5-COD)Ir·P$_2$W$_{15}$Nb$_3$O$_{62}$] (**1**) (1.44 μmol **1** in 9.0 mL of acetone plus 9.0 mL of cyclohexene) at 22 °C and 40 ± 1 psig H$_2$.

Nb$_3$O$_{62}$] and [(1,5-COD)Ir(CH$_3$CN)$_2$]BF$_4$ according to eq 1 and under Standard Conditions gives the same results for the five tests as those obtained with the preformed, isolated, and purified complex, [Bu$_4$N]$_5$Na$_3$[(1,5-COD)Ir·P$_2$W$_{15}$Nb$_3$O$_{62}$], **1**. If the same results can be obtained with the easier and quicker in situ method, then the important, time-saving advantage is that it becomes unnecessary for us, or others, to synthesize, isolate, and characterize *each* precatalyst complex for *all* anions or other stabilizers of interest—just to then go on and break apart the metal—ligand bonds in that complex en route to nanoclusters. Note, however, that the isolated precatalyst (e.g., **1**) approach provides exact control over the metal-to-stabilizer stoichiometry, an important consideration in the nucleation and growth steps, and thus the reason we started our studies with that more demanding, slower approach[25,26,28]—which yielded the important reference point of ±15% reproducibility in nanocluster properties.[25,26,28] Note, then, that four differences between the in situ and preisolated complex methods are as follows: the level of control over the metal-to-stabilizer stoichiometry; the reaction time used to form the complex in the in situ experiment (i.e., is the time chosen sufficient for complete formation of the complex?); the lack of any purification step in the in situ method and, hence, the presence of the Bu$_4$N$^+$BF$_4^-$ byproduct, ([Bu$_4$N]$_9$[P$_2$W$_{15}$Nb$_3$O$_{62}$] + [(1,5-COD)Ir(CH$_3$CN)$_2$]BF$_4$ → **1** + Bu$_4$N$^+$BF$_4^-$); but, again, the much greater ease and rapidity of doing experiments by the (therefore highly desirable) in situ method.

Fortunately, the results in Table 1, entry 2, and in comparison to entry 1, *show that the in situ method can be used with essentially the same results*. A Standard Conditions synthesis and hydrogenation reaction starting with 1.2 mM [Bu$_4$N]$_9$-[P$_2$W$_{15}$Nb$_3$O$_{62}$] and 1.2 mM [(1,5-COD)Ir(CH$_3$CN)$_2$]BF$_4$ gave a typical sigmoidal hydrogen loss versus time curve (Figure S-2, Supporting Information). The resultant induction period, $-d[H_2]/dt$ rate, k_1, k_2, and other measurables are close to, and in most cases probably within 3σ experimental error of, those obtained for **1** (compare the columns in Table 1 for entries 1 and 2; see also the TTOs plot yielding 51 000 TTOs over 10 days in Figure S-3 of the Supporting Information). The small, apparent 2-fold difference in the sensitive[28,50] k_1 value is probably real, reflecting the high sensitivity of the nucleation reaction to traces of the solvate[28,50] [(1,5-COD)Ir(CH$_3$CN)$_2$]$^+$—one reason this control experiment is not trivial. The variation in k_1 may also reflect the fact that the two starting solutions do

not have the exact same composition (the in situ experiment of 1.2 mM $[Bu_4N]_9[P_2W_{15}Nb_3O_{62}]$ plus 1.2 mM $[(1,5\text{-}COD)Ir(CH_3CN)_2]BF_4$ contains 2 equiv of CH_3CN, 1 equiv of BF_4^-, and 4 equiv of Bu_4N^+ instead of 3 equiv of Na^+ as in the solution of 1.2 mM **1**). Fortunately, however, for the comparative studies herein any such small differences between starting with isolated **1** vs its in situ components should be negligible, *especially since the data for all anions in Table 1 have been obtained by the same, directly comparable, in situ precursor method.*

Controls Adding OH⁻: The $P_2W_{15}Nb_3O_{62}^{9-}$ Polyoxoanion and Its Comparison to the Nb−O−Nb Bridged Anhydride Polyoxoanion, $[(P_2W_{15}Nb_3O_{61})_2O]^{16-}$. Three additional, important controls were done: first, a control was done testing whether adding 1 equiv of $Bu_4N^+OH^-$ *at the start of the reaction* to scavenge the H^+ formed, eq 1, thereby yielding $P_2W_{15}Nb_3O_{62}^{9-}$ as the resultant stabilizer, significantly improves the nanocluster formation and stabilization. Table 1, entry 3 shows that although the initial kinetic control is increased some $(k_2/k_1 = 5.0(4) \times 10^5$, a value 2.6-fold higher than entries 1 or 2 in Table 1), the key ability to redissolve the nanoclusters and the 4-fold reduced TTO catalytic lifetime are inferior to when no OH^- is added (Table 1, entries 1 and 2). (Figures S-4, S-5, and S-6 in the Supporting Information present respectively the kinetic curve, TTO, and TEM data for this control.) Note here that since $Bu_4N^+OH^-$ was added at the start of the reaction there is excess OH^- present until the very end of the reaction since H^+ is produced only piecemeal as the reaction proceeds. *The key, more than 300, nanocluster nucleation and growth steps[28] are, therefore, done in the presence of OH^-.* Hence, a second control experiment probing any effects of *the timing of the addition of OH^-* was done: 1 equiv of $Bu_4N^+OH^-$ was added into the solution *after* the formation of the nanoclusters but in an otherwise identical Standard Conditions experiment; a second hydrogenation experiment (1.6 M cyclohexene; 40 psig H_2) was then performed. The results were similar: black particles are again observed implying poorer nanocluster stabilization in this experiment. A third control experiment was also done adding 1 equiv of $Bu_4N^+OH^-$ at the *start* of an *in situ generation* of the nanoclusters, entry 4, Table 1. This experiment again produced insoluble black particles. Ultracentrifugation (Figure S-1, top half) confirmed that the expected, monomeric $P_2W_{15}Nb_3O_{62}^{9-}$ is the nanocluster stabilizer species present when 1 equiv of base is added.

In short, the addition of OH^- to scavenge the H^+ formed via eq 1 does not yield improved nanocluster formation and stabilization in at least the above case nor, as we shall see, those of the other anions examined below. We are, however, finding some interesting effects of other less strong/less coordinating bases using the methods and five criteria developed herein, results which are detailed elsewhere.[32]

The Citrate Anion, $C_6H_5O_7^{3-}$. The citrate trianion, $C_6H_5O_7^{3-}$, has been a very common, *combined* reducing and stabilizing agent in nanocolloid chemistry[37−39] since the time of Turkevich's early work.[38] It is arguably the current, de facto "Gold Standard" among nanocluster stabilizing anions. Despite the common use of citrate to stabilize nanoclusters, its binding mode in even simple complexes is little studied. There is one crystal structure,[51] that of $[Fe(C_6H_8O_7)_2]^{5-}$, showing that citrate can bind via a facial array of three oxygen atoms, a situation very similar to the polyoxoanions discussed already. Citrate has, however, one significant disadvantage that is clear from Turkevich's pioneering work,[38b] a disadvantage that is almost never discussed in current work employing citrate: citrate is a reagent (a reductant) as well as a stabilizer. That is, citrate is a non-innocent ligand, becoming oxidized to the intermediate ketone (acetone dicarboxylic acid), which in turn is an even better (autocatalytic[38b]) reducing agent. This reaction results in two undesirable features: a less controlled, or controllable, complex stoichiometry for the all-important nucleation reaction, plus the production of a complex mixture of compositionally ill-defined stabilizing agents, including any remaining citrate. The unavoidable result is a compositionally ill-defined, nano-*colloid* (following the nanocluster vs nanocolloid definitions and distinctions given elsewhere[2]). In addition, there is no idea whatsoever in the prior literature of how citrate stacks up fundamentally in its ability to allow a high level of kinetic control in nanocluster syntheses, to allow isolable nanoclusters without bulk metal formation, or to provide nanoclusters with high catalytic rates and long lifetimes. Hence, it is of considerable interest to examine this prior "de facto Gold Standard" anion by the five criteria.

The needed experiments were accomplished by using a Standard Conditions nanocluster synthesis and 1.6 M cyclohexene hydrogenation experiment beginning with 1.2 mM $[Bu_4N]_3[C_6H_5O_7]$ and 1.2 mM $[(1,5\text{-}COD)Ir(CH_3CN)_2]BF_4$ in acetone at 22 °C; a yellow to orange color change is seen as soon as the citrate is added to solution, suggestive of the formation of a complex between $(1,5\text{-}COD)Ir^+$ and $(citrate)^{3-}$. A *roughly* sigmoidal cyclohexene loss vs time curve is seen, Figure 5, but it is clearly different than any seen in this work, or any that we have seen previously,[2,28,26] in that it exhibits a descending linear portion in the initial induction period (i.e., instead of the typically observed, horizontal-line induction period) followed by the usual, approximately linear H_2 uptake. It is clear from just this initial portion of the kinetic curve that *there is another pathway for nucleation over and above the one normally seen* with H_2 as a reductant. This added kinetic path is most likely either the citrate-as-a-reductant pathway noted by Turkevich[38b] (e.g., via the $(1,5\text{-}COD)Ir^+/(citrate)^{3-}$ complex noted above) or a contribution by some other, different nucleation mechanism when citrate is present. Even without further data or analysis one can see that this aspect of citrate is undesirable: it results in a smaller separation of nucleation and growth in time, and thus less kinetic control in the nanocluster synthesis, plus a complex, ill-defined mixture of citrate-derived products as possible stabilizers.

A smaller k_2/k_1 ratio is confirmed by the data summarized in Table 1, entry 5, the k_2/k_1 is 0.50(5) $\times 10^5$ M⁻¹, a value 4-fold

(50) Noteworthy here is that the $k_1 = 0.015(1)$ h⁻¹ value measured herein for **1** is almost an order of magnitude larger than the value previously measured under similar conditions by an earlier worker in our group, $k_1 = 0.0018(1)$ h⁻¹.[28a] Typically, the agreement in k_1 values is much better than this (7 repeat experiments showed that the k_1 for **1** is reproducible to ±30% for the studies reported herein), but our earlier work[26,28] shows that the induction period and its associated k_1 value is, indeed, *very sensitive* to the exact conditions, the source and purity of the acetone, traces of water, the H_2 pressure, and especially traces of Ir(1,5-COD)⁺. One likely possibility is that this discrepancy reflects a small variation in the exact Ir(1,5-COD)⁺ to $P_2W_{15}Nb_3O_{62}^{9-}$ ratio in the precursor **1** used in the two studies. For this reason, we made every effort to weigh carefully, and thereby control the exact Ir(1,5-COD)⁺ to anion ratio used in the present study.

(51) The only example of an isolated mononuclear transition metal citrate complex that we could find: Matzapetakis, M.; Raptopoulou, C. P.; Tsohos, A.; Papaefthymiou, V.; Moon. N.; Salifoglou, A. *J. Am. Chem. Soc.* **1998**, *120*, 13266.
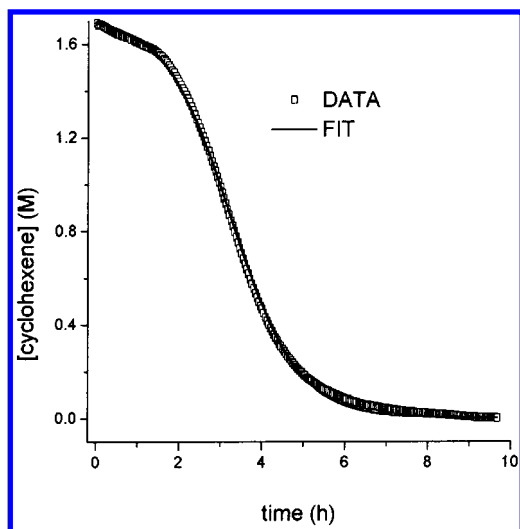
Figure 5. Cyclohexene loss vs time data and curve-fit for the hydrogenation of 1.6 M cyclohexene and concomitant formation of 23 ± 5 Å Ir(0) nanoclusters starting with 1.2 mM [Bu$_4$N]$_3$[C$_6$H$_5$O$_7$] and 1.2 mM [(1,5-COD)Ir(CH$_3$CN)$_2$]BF$_4$ in acetone at 22 °C. Note the *initially descending*, rather than typically flat, line seen in the first part of the curve, results which strongly suggest a second nucleation pathway when citrate is present in addition to the normal nucleation[28] pathway.

smaller than that for the [(P$_2$W$_{15}$Nb$_3$O$_{61}$)$_2$O]$^{16-}$ polyoxoanions (entries 1 vs 5 Table 1); note that the *apparent* k_1 for citrate must be a composite of the ≥ 2 nucleation pathways. Also, as predicted from the smaller k_2/k_1 ratio, the distribution in the resultant black residue is somewhat broader than near-mono-disperse $(\pm 15\%)^2$, namely 23 ± 5 Å $(\pm 22\%)$, Figure 6. Significantly, the resultant nanoclusters *cannot* be redissolved without the formation of some bulk metal (Table 1, entry 5, column 9), implying a lower level of stabilization by citrate. A 4.7-fold slower catalytic activity for the resultant combined nanocluster/bulk metal material is also seen (column 10) along with 43 000 TTOs (Figure S-7 of the Supporting Information).

A control adding 1 equiv of Bu$_4$N$^+$OH$^-$ at the start of the reaction proved important and adds further support to the claim herein that attention to the stoichiometry in eq 1 and the production of 1 equiv of H$^+$ can no longer be ignored: the resultant cyclohexene loss curve *cannot* be fit by the normal A → B, A + B → 2B kinetic scheme. Instead, following a 0.2(1) h induction period, the curve starts abruptly with a fast hydrogenation which slows down after 50% conversion (Figure S-8 of the Supporting Information). Clearly a different nano-cluster formation mechanism is operative in this case. Interest-ingly, the resultant nanoclusters are now fully redissolvable, but they show a somewhat broad, 22 ± 5 Å $(\pm 23\%)$ distribution with obvious agglomeration (Figure S-9 of the Supporting Information) and undergo only 12 000 TTOs over 2 days before deactivation (Table 1, entry 6), a value 4.3 times lower than the best polyoxoanion entry of 51 000 (entry 2, Table 1).

These results provide the first quantitative analysis of the relative ability of citrate to allow the preparation, and then stabilization, of transition-metal nanoclusters. At least for Ir(0) nanoclusters, *citrate is clearly inferior to the [(P$_2$W$_{15}$Nb$_3$O$_{61}$)$_2$O]$^{16-}$ polyoxoanion by each of the five criteria* (entries 1−3 vs 5−6, Table 1), so that the developing anion series is [(P$_2$W$_{15}$Nb$_3$O$_{61}$)$_2$O]$^{16-}$ > C$_6$H$_5$O$_7^{3-}$.

Polyacrylate Anion, [−CH$_2$-CH(CO$_2^-$)−]$_n^{n-}$. Poly(acrylic acid) as its Na$^+$ salt has been used as a polymeric stabilizer for
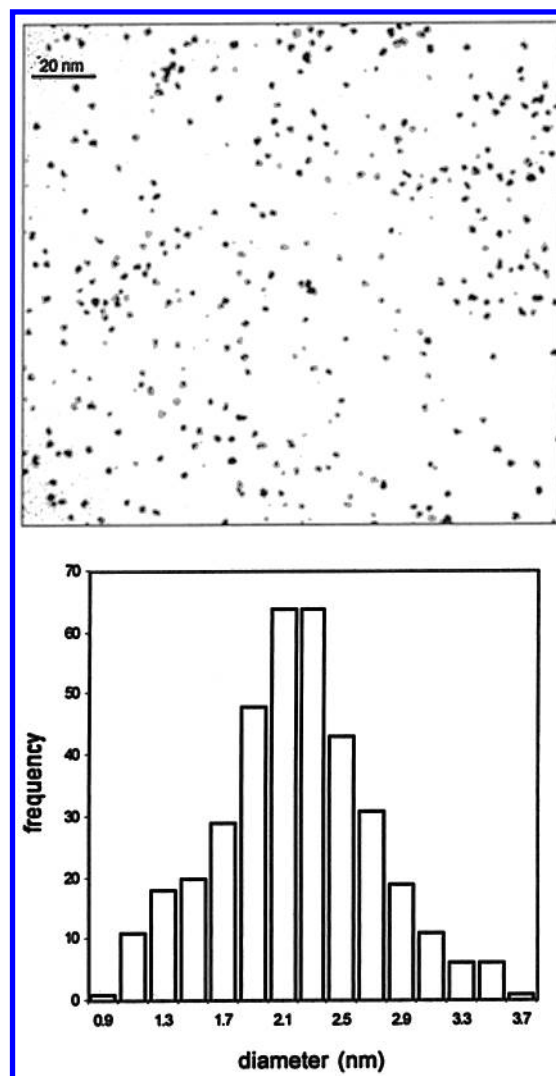

Figure 6. TEM image (430 K magnification) and the associated particle size histogram (367 nontouching particles counted by NIH Image) of isolated 23 ± 5 Å Ir(0)$_{\sim 300}$ nanoclusters grown by hydrogen reduction of 1.2 mM [(1,5-COD)Ir(CH$_3$CN)$_2$]BF$_4$ with 1.2 mM [Bu$_4$N]$_3$[C$_6$H$_5$O$_7$] in acetone under Standard Conditions described in the Experimental Section. The sample was harvested after 10 h of hydrogenation since bulk metal had already precipitated by that time.

the platinum nanoparticles in aqueous media;[40] the interesting but unanswered question here is whether poly-carboxylates are as good a stabilizer as their polyanionic character and common use seem to suggest.

The needed studies were accomplished by preparing the Bu$_4$N$^+$ salt from commercially available poly(acrylic acid) (MW 2000) plus Bu$_4$NOH in acetone with added, predried 5 Å mol sieves to remove as much as possible the water generated or present initially (see the Experimental Section for details). Note here that the contributions by water in the polyacrylate to both the nanocluster formation reaction and the nanocluster (de)-stabilization[26,28a] are issues that have received little prior attention but merit consideration whenever polyacrylate and other hydrophilic polymeric stabilizers are used.

Two otherwise Standard Condition nanocluster syntheses and concomitant cyclohexene hydrogenation experiments were performed starting with 1.2 mM [(1,5-COD)Ir(CH$_3$CN)$_2$]BF$_4$ plus 1.2 mM (and in the second experiment, 6.0 mM) [−CH$_2$-CH(CO$_2^-$)−]$_n$[Bu$_4$N]$_n$, in acetone at 22 °C. In both cases the
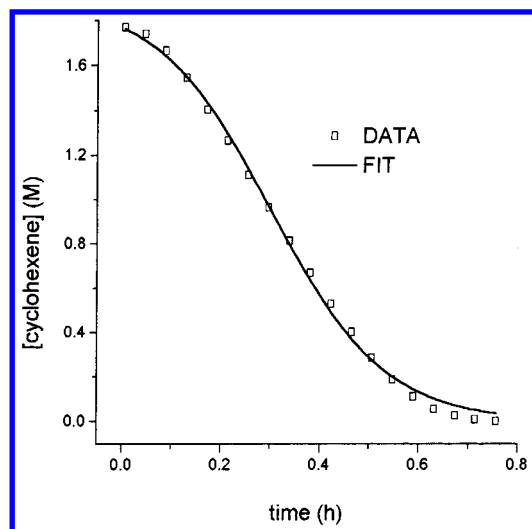
Figure 7. Cyclohexene loss vs time data and curve-fit for the hydrogenation of 1.6 M cyclohexene starting with 1.2 mM poly(acrylic acid), as its tetrabutylammonium salt, and 1.2 mM [(1,5-COD)Ir(CH$_3$CN)$_2$]BF$_4$ in acetone at 22 °C. Note that the reaction proceeds quickly after a short induction period of only ca. 0.1(1) h, indicating a low level of kinetic control in this nanocluster formation reaction.

concentration of stabilizer is given as the molarity of $-CO_2^-$ groups present so that it is directly comparable to the concentrations of monomeric stabilizers. The cyclohexene loss vs time curves are given in Figure 7 and Figure S-10 of the Supporting Information; for both 1.2 and 6.0 mM poly(acrylic acid) the hydrogenation proceeds with only a slight induction period (ca. 0.1 h) so that the resultant k_1 values are large, $k_1 = 0.60(5)$ h^{-1} and $k_1 = 1.1(1)$ h^{-1}, respectively (Table 1, entries 7 and 8). Hence, the observed k_2/k_1 values are still ≥20-fold smaller than those for the [(P$_2$W$_{15}$Nb$_3$O$_{61}$)$_2$O]$^{16-}$ polyoxoanion, for example, entry 1 in Table 1. *A relatively low level of kinetic control of nanocluster formation by polyacrylate is implied, a previously unavailable insight.*

In the experiment with 1.2 mM [$-$CH$_2$-CH(CO$_2^-$)$-$]$_n$-[Bu$_4$N]$_n$, black bulk metal precipitates resulting in a *clear*, essentially metal-free solution after 5 h. With 6.0 mM (5 equiv) of polyacrylate per each iridium atom initially present the solution turns brown (indicating some soluble nanoparticles) rather than clear, but bulk metal still precipitates after 5 h in the form of very fine particles. In even this latter experiment, the residue obtained after removing the volatiles under vacuum is only partly redispersable in acetone (Table 1, entry 8). The kinetic and other data place polyacrylate below citrate^{3-} in the developing anion series: [(P$_2$W$_{15}$Nb$_3$O$_{61}$)$_2$O]$^{16-}$ > C$_6$H$_5$O$_7^{3-}$ > [$-$CH$_2$-CH(CO$_2^-$)$-$]$_n^{n-}$.

Chloride Anion, Cl$^-$. Chloride anion is perhaps the *most common*,[36] but previously unranked, nanocluster stabilizer. Note that in this experiment we started with the preformed complex [(1,5-COD)IrCl]$_2$ rather than [(1,5-COD)Ir(CH$_3$CN)$_2$]BF$_4$ plus Bu$_4$NCl, since the latter, in situ mixture will just quickly reform [(1,5-COD)IrCl]$_2$. Recall that [(1,5-COD)Ir(CH$_3$CN)$_2$]BF$_4$ is made from [(1,5-COD)IrCl]$_2$ plus AgBF$_4$ as detailed in the Experimental Section; note also that one difference vs earlier experiments is that no Bu$_4$N$^+$BF$_4^-$ is present, so that this experiment probes Cl$^-$ stabilization in the absence of any additional stabilization provided by Bu$_4$N$^+$. Entry 9 of Table 1 shows the results of a Standard Conditions experiment starting with 0.6 mM [(1,5-COD)IrCl]$_2$ (i.e., 1.2 mM in Ir) in acetone
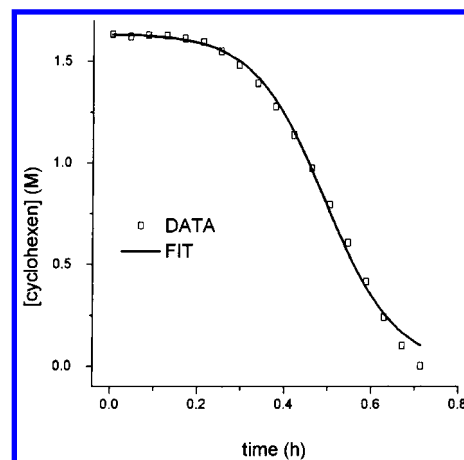

Figure 8. Cyclohexene loss vs time data and curve-fit for the hydrogenation of 1.6 M cyclohexene starting with 0.6 mM [(1,5-COD)IrCl]$_2$ in acetone at 22 °C. An induction period of 0.2(1) h is followed by a fast reaction corresponding to $-$d[cyclohexene]/d$t = -$d[H$_2$]/d$t = 12(1)$ mmolH$_2$/h. Hydrogen uptake continues after the cyclohexene to cyclohexane conversion as can begin to be seen by the poor curve-fit toward the end of reaction. This secondary H$_2$-uptake reaction has been shown to be acetone hydrogenation in the presence of the H$^+$Cl$^-$ formed in the nanocluster synthesis reaction, the details of which will be reported elsewhere.[52]

at 22 °C; a sigmoidal cyclohexene loss vs time curve is seen, Figure 8, one well fit by the nucleation plus autocatalytic surface growth mechanism until the very end, at which point *hydrogen uptake still continues*. This further hydrogen uptake has been studied separately and is due to a facile hydrogenation of the acetone solvent and in the presence of the 1 equiv of HCl generated by the nanocluster formation reaction, an interesting finding in its own right that will be reported in greater detail elsewhere.[52] The curve-fit and resultant k_1 and k_2 values give a relatively large $k_2/k_1 = 3.6(7) \times 10^5$ (Table 1 entry 9), implying a high level of kinetic control in the initial nanocluster formation reaction, a level 1.9-fold higher than that seen for the [(P$_2$W$_{15}$Nb$_3$O$_{61}$)$_2$O]$^{16-}$ polyoxoanion (Table 1, entries 1 and 2), but 1.4-fold less than the polyoxoanion with added OH$^-$ (entry 3). However, as the hydrogenation reaction employing [(1,5-COD)IrCl]$_2$ proceeds, the yellow solution becomes colorless with the formation of very fine black particles of bulk metal in the bottom of the reaction tube—that is, the stabilization is insufficient to prevent bulk Ir(0) metal formation.

Recall that Bradley's literature[44b] shows that the uncontrolled production of H$^+$Cl$^-$ in nanoparticle synthesis reactions yields nanoparticles with quite variable catalytic rates; hence, we added 1 equiv of Bu$_4$N$^+$OH$^-$ to scavenge the H$^+$Cl$^-$ making the resultant stabilizer the significantly more basic Bu$_4$N$^+$Cl$^-$, an experiment that also adds back any Bu$_4$N$^+$ stabilization effects. Figure 9 shows a typical curve fit of the cyclohexene loss vs time in the cyclohexene hydrogenation starting with 0.6 mM [(1,5-COD)IrCl]$_2$ (i.e., 1.2 mM in Ir) and 1.2 mM Bu$_4$NOH in acetone at 22 °C. The clear orange solution still turns colorless with *precipitation of black bulk metal* within 1 h. The curve in Figure 9 is rather different than the one in Figure 8 with, for example, a shorter induction period of 0.1(1) h and an associated larger $k_1 = 0.30(1)$ h^{-1} and smaller k_2/k_1 of $4.7(4) \times 10^4$ (Table 1, entry 10), that is, ca. 4-fold less kinetic control over

(52) The facile hydrogenation of acetone by nanoclusters formed from [(1,5-COD)IrCl]$_2$ (plus the H$^+$Cl$^-$ generated in the reaction) will be reported in a separate paper: Özkar, S.; Finke, R. G. Unpublished results and experiments in progress.
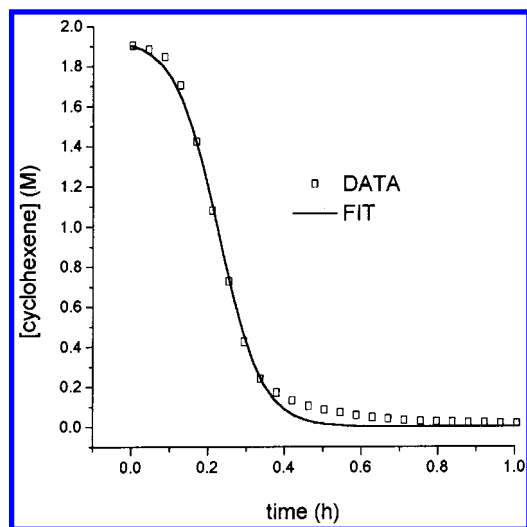
Figure 9. Cyclohexene loss vs time data and curve-fit for the hydrogenation of 1.6 M cyclohexene starting with 0.6 mM [(1,5-COD)IrCl]$_2$ and 1.2 mM Bu$_4$NOH in acetone at 22 °C. A short induction period of 0.1(1) h indicates that there is relatively little kinetic control in the nanocluster synthesis reaction, while the poor curve-fit toward the end of reaction is suggestive of Ir(0) agglomeration to form bulk metal (precipitation of bulk metal is in fact observed; see Table 1, entry 10).

nanocluster formation than seen for the [(P$_2$W$_{15}$Nb$_3$O$_{61}$)$_2$O]$^{16-}$ polyoxoanion (Table 1, entries 1 and 2) and a 7.6-fold lower k_2/k_1 value vs the experiment without added Bu$_4$N$^+$OH$^-$ (entry 9, Table 1). In addition, the curve fit at longer reaction times in Figure 9 errors on the low side of the observed data, a feature that is consistent with agglomeration of Ir(0) to lower surface area (and thus less reactive) bulk metal particles (which, therefore, show a rate less than the calculated curve fit). The results place Cl$^-$ at the end of the developing anion series along with polyacrylate: [(P$_2$W$_{15}$Nb$_3$O$_{61}$)$_2$O]$^{16-}$ > C$_6$H$_5$O$_7$$^{3-}$ > [−CH$_2$-CH(CO$_2$$^-$)−]$_n$$^{n-}$ ∼ Cl$^-$ (chloride's better k_2/k_1 ratio being offset by polyacrylate's better (partial) redissolvability).

Summary and Conclusions

The following are the major findings of the present study, the first study of its kind establishing and then using modern criteria for rating common anions for their nanocluster formation and stabilizing abilities:

(1) The *methods* and *five criteria* were developed and are now available for more widespread use, results which build vertically off of our earlier studies of the synthesis, characterization, mechanism of formation, and mechanisms of stabilization of polyoxoanion- and tetrabutylammonium-stabilized transition-metal nanoclusters.[2,25,26,28] The methods include the in situ use of [(1,5-COD)Ir(CH$_3$CN)$_2$]$^+$ with [Bu$_4$N]$_q$Y (and, by implication other metals or precursors), and the pseudoelementary step kinetic method[28] to follow the nanocluster growth via large amounts of high-precision H$_2$-uptake data. The five criteria will allow the efficacy of nanocluster stabilizing solvents, cations, polymers, and other additives[35] to be examined in the future as well as the anions studied as part of this first study. Also noteworthy is that the five criteria both address *and separate* nanocluster formation and stabilization for the first time. In addition the data obtained support the conclusion that the nanocluster A → B, A + B → 2B formation mechanism, and thus k_2/k_1 criteria are generally applicable to transition-metal nanoclusters formed under H$_2$.[28]

(2) The important, literature-correcting[13] insight was provided showing that the *anion* is the first crucial and fundamental component of stabilization of at least uncharged, neutral core, transition-metal M(0)$_n$ nanoparticles. Still needed, however, are analogous systematic studies of a range of solvents, cations, and polymers of various chain lengths; such studies are in progress.[35]

(3) The first *anion series* was provided: [(P$_2$W$_{15}$Nb$_3$O$_{61}$)$_2$O]$^{16-}$ > C$_6$H$_5$O$_7$$^{3-}$ > [-CH$_2$−CH(CO$_2$$^-$)-]$_n$$^{n-}$ ∼ Cl$^-$. *Note that this series applies, strictly speaking, only to the Ir(0) nanoclusters for which it was measured and in acetone solvent with Bu$_4$N$^+$ as the common countercation.* We note here that it remains to be seen to what extent an absolute anion series does, or does not, result: *one is not necessarily anticipated* since effects, such as a matching of the anion's chelating atoms and the surface metal's lattice[33] as well as hard and soft acid and base considerations (or as the surface metal's oxidation state changes), promise to be important in determining the anion series for other metals and situations. Literature Pd(0) nanoclusters, for example, often are made with Cl$^-$ and Br$^-$ as apparently preferred,[13,15,24] but rigorously unranked, stabilizers. The present studies are, then, just the beginning of needed investigations determining the anion series for Pd(0), Pt(0), Rh(0), Ru(0) and other nanoclusters.

(4) Highly charged, basic polyoxoanions such as [(P$_2$W$_{15}$-Nb$_3$O$_{61}$)$_2$O]$^{16-}$ were established as the present Gold Standard of transition-metal stabilizing anions, again at least for Ir(0) nanoclusters in acetone and with Bu$_4$N$^+$ as the countercation. This finding's greatest significance is that it provides a previously unavailable *focal point* for future studies, work that should now be considerably more focused and efficient as it strives to design, then quickly test, even better anions for nanocluster syntheses and stabilization. We note here that there is also a need to define the attributes of the "Gold Standard" stabilizers for nanoclusters focused toward optical, electronic, magnetic, and other properties different from the catalytic properties emphasized in the present work.

(5) The correction was provided of the previous beliefs that polyacrylate or Cl$^-$ are superior stabilizers, or that citrate^{3-} is the Gold Standard among known anionic stabilizers, at least for Ir(0) nanoclusters in acetone with Bu$_4$N$^+$ counterions. Also noteworthy are the issues discussed due to citrate functioning as both a reductant and as a stabilizer, issues first articulated in Turkevich's classic work,[37,38] and issues supported by the findings herein, notably the kinetic evidence that citrate serves as a reductant, with the result being ≥2 nucleation pathways, even under 40 psig H$_2$.

(6) Data were provided extending the finding of the *greater generality* of the A → B, rate constant k_1, then A + B → 2B, rate constant k_2, *slow and continuous nucleation and then fast autocatalytic surface-growth mechanism* of transition-metal nanoparticle formation under H$_2$.[28] Having this mechanism available to guide nanoparticle syntheses is continuing to prove very valuable.[2,53]

(53) Yu, H.; Gibbons, P. C.; Kelton, K. F.; Buhro, W. E. Heterogeneous Seeded Growth: A Potentially General Synthesis of Monodisperse Metallic Nanoparticles. In *J. Am. Chem. Soc.* **2001**, *123*, 9198. This interesting work extends the generality of the surface autocatalytic growth mechanism[28] by showing that Bi, Sn, or In nanoparticles can be grown on Au seeds and from the higher temperature decomposition of Bi[N(SiMe$_3$)$_2$]$_3$, Sn(NMe$_2$)$_2$, and In(C$_5$H$_5$).

(7) Data were provided illustrating and extending the finding[28b] that the k_2/k_1 ratio is the present, best kinetic handle for predicting the level of kinetic control and for predicting how close (or far) from near-monodisperse a given transition-metal nanocluster synthesis is, *initially*. Larger values signify one of the two limits of greater separation of nucleation and growth in time and, therefore, an increasing tendency toward narrower size-distributions of nanoclusters. Those using the k_2/k_1 ratio rather than its more rigorous $k_2[B]/k_1$ counterpart will, however, wish to be familiar with the discussion and points made in a section of the Supporting Information: A Closer Look at the Proper Use of the k_2/k_1 Ratio and Its Two Interesting Limits, Large vs Small k_2/k_1 Ratios.

(8) And, evidence was provided that added base, to scavenge the H^+ generated according to eq 1, is an important variable that can influence both the nanocluster formation (e.g., entries 8 and 9 in Table 1 corresponding to Figures 5 and 6) or nanocluster isolability and catalytic lifetime (entries 1 vs 3, Table 1). Studies of other bases are needed, however, and are in progress.[32,35]

Overall, the present work provides a foundation from which to begin to probe more deeply, and to better understand, which anions, cations, solvent, and polymers or oligomers provide which transition-metal nanoclusters with the best kinetically controlled syntheses, stabilization, and desired physical properties.

Experimental Section

Materials. All commercially obtained compounds were used as received unless indicated otherwise: acetone was purchased from Burdick & Jackson (water content <0.2%) and was purged with argon and transferred into a nitrogen atmospheres drybox before use. It is known that the source and H_2O content of the acetone both matter for reproducible nanocluster syntheses.[26] Cyclohexene (Aldrich, 99%) was purified by distillation over sodium under argon and stored in the drybox. Aqueous $Bu_4N^+OH^-$ solutions (40% in water, Aldrich, freshly opened) were titrated separately with 0.1 M HCl to methyl red and phenolphthalein end points (i.e., for both amine and total base content) immediately prior to use. $AgBF_4$ (Aldrich, purified by extraction with diethyl ether followed by evaporation of the extract under vacuum to give a white powder). Solutions of Bu_4NOH in acetone were made up fresh and should not stand for long periods of time due to aldol condensation reactions and different, enhanced catalytic rates from older solutions that we have seen in both the present work and earlier work (see Table B and Figure G in Supporting Materials elsewhere[26]). Poly-(acrylic acid) (Aldrich; MW 2000) was used as received. Deuterated NMR solvents CD_3CN and CD_2Cl_2 (Cambridge Isotope Laboratories) were received in 1 mL glass ampules which were transferred into the drybox for NMR sample preparation done in the drybox. The nanocluster precursor complexes $[Bu_4N]_5Na_3[(1,5\text{-}COD)Ir\cdot P_2W_{15}\text{-}Nb_3O_{62}]$[54] and $[Bu_4N]_9[P_2W_{15}Nb_3O_{62}]$ were made by our most recent method[41] and then stored in the drybox. The iridium solvate complex, $[(1,5\text{-}COD)Ir(NCCH_3)_2]BF_4$, was prepared according to the procedure for the corresponding hexafluorophosphate salt.[55] Purity of these complexes was checked by ^1H, ^{13}C, and ^{31}P NMR spectroscopy.

Hydrogenations. All the nanocluster formation and hydrogenation reactions were carried out on the previously described,[26,28a] custom-built pressurized hydrogenation apparatus. Full details are reported in the Supporting Information under the identical heading, "Hydrogenations".

Curve Fits of the Hydrogen Uptake Data and Data Handling. Data handling and curve fitting of the H_2 pressure (or, equivalently, the cyclohexene loss) vs time data were performed, as described previously,[28d] with the software package Microcal Origin 3.54 with its nonlinear regression subroutine (RLIN) and modified Levenberg-Macquardt algorithm.[56] (Details of both procedures are available in Supporting Information under the same heading.) Error bars are provided in Table 1 and are typically $\leq\pm15-20\%$ (except for k_1, where somewhat larger errors are the norm; see footnote 50). Error bars on data are not shown in the figures to avoid cluttering them.

Transmission Electron Microscopy (TEM): Sample Preparation. The solutions used for the TEM experiments were the exact same ones prepared below in the Standard Conditions and the Catalytic Lifetime Experiments sections. However, at the end of a given run (i.e. at a minimum time required for the complete formation of nanoclusters as determined by the cyclooctane evolution in the Standard Conditions hydrogenation and at the end of the catalytic lifetime experiments), the Fischer−Porter (F−P) bottle was detached from the hydrogenation line via its quick-connects and brought back into the drybox, and its acetone solution was quantitatively transferred with a disposable polyethylene pipet into a clean, 5 mL screw-capped glass vial. The solution was dried under vacuum and the glass vial was then sealed and brought out of the drybox. The dry nanocluster samples in screw-capped glass vials were sent as solids to the University of Oregon for TEM investigation. There, 1 mL of acetonitrile was added, in air, just before a TEM was obtained, to yield a clear amber, homogeneous solution (in general, no bulk metal was visible by the naked eye at any time unless otherwise indicated). A drop of this solution was then dispersed on a chloroform-cleaned, carbon-coated Cu TEM grid.

Sample TEM Analyses. TEM analyses were performed as before[28a,26] at the University of Oregon with the expert assistance of Dr. Eric Schabtach, using the sample preparation procedure and a Philips CM-12 TEM with a 70 μm lens operating at 100 kV and with a 2.0 Å point-to-point resolution, as described in detail previously.[25] Typically, TEM pictures of each sample were taken at three different magnifications (100-, 200-, and 430K) to obtain information about the sample in general (100K), plus a closer visualization of the clusters (430K). A number of control experiments were done previously which provided good evidence that results are truly representative of the sample (i.e., save any crystallization in the electron beam) and that the sample is not otherwise perturbed by application of the TEM beam [e.g., controls showing that varying the sample spraying method (in air or under N_2) or depositing the sample as a drop and letting it dry did not change the results; controls showing that changing the beam voltage from 40 to 100 kV, or changing the exposure time (seconds vs minutes), did not change the images; other controls have been done as well].[25]

Particle Size Measurements. Particle size analysis was performed with use of the public domain NIH Image 1.62 program (available on the Internet at http://rsb.info.nih.gov/NIH Image/). The following steps were taken to prepare the data for analysis: (i) A bright field TEM image was obtained with even illumination. Images were chosen to be as representative of the bulk sample as possible. (ii) The image was then scanned into a computer using a scanning camera (Lumina) for the negative and saved as a TIFF file. (iii) Using Adobe PhotoShop, the contrast/brightness and channel curves were adjusted so that particles stand out clearly from the background. This is the most difficult for small particles, which inherently have less contrast. In NIH Image 1.62, after having set the scale and the threshold, the "Analyze Particles" feature was used to generate a table of particle areas and diameters (major and minor axes). This table was then exported into Microsoft Excel 98 where histograms, statistical analysis, and histogram plotting were performed. For each particle, the diameter was calculated from the area by assuming that the nanoclusters are circular. Size distributions are quoted as the mean diameter $\pm$ the standard deviation.

(54) Pohl, M.; Lyon, D. K.; Mizuno, N.; Nomiya, K.; Finke, R. G. *Inorg. Chem.* **1995**, *34*, 1413.
(55) Day, V. W.; Klemperer, W. G.; Main, D. J. *Inorg. Chem.* **1990**, *29*, 2343 and references therein.

(56) Press, W. H.; Flannery, B. P.; Teukolsky, S. A.; Vetterling, W. T. *Numerical Recipes*; Cambridge University: Cambridge, 1989.

Nanocluster Formation and Cyclohexene Hydrogenations (Standard Conditions). These experiments were performed by following closely our established protocol.[26,28a] Briefly, in the nitrogen-filled drybox, 3.6 ± 0.2 μmol of the precatalyst material was dissolved in 2.5 mL of acetone (added via a 5.0 mL gastight syringe) in a disposable 2-dram glass vial. Cyclohexene (0.5 mL, 4.94 mmol) was added to the solution with use of a 1.0 mL gastight syringe. The resultant clear, homogeneous solution was transferred via a disposable polyethylene pipet into a new 22×175 mm Pyrex culture tube containing a new $5/16 \times 5/8$ in. Teflon-coated stir bar. The culture tube was then sealed inside of the F—P pressure bottle, brought outside of the drybox, placed inside a constant temperature circulating bath at 22.0 ± 0.1 °C, and attached via Swagelock TFE-sealed quick-connects to the hydrogenation line (which had already been evacuated for at least 30 min to remove any trace oxygen and water present, then refilled with purified H_2 at 40 ± 1 psig). Stirring was started (at >600 rpm) and the F—P bottle was then purged 15 times with hydrogen (15 s per purge) and stirred vigorously for an additional 30 s, then $t = 0$ was started. Hydrogen pressure in the F—P bottle was then monitored as a function of time via the computer-interfaced pressure transducer.

After a minimum time required for the complete formation of nanoclusters as determined by a cyclooctane evolution experiment, the hydrogenation was stopped and the F—P bottle was sealed, disconnected from the hydrogenation line, and transferred into the drybox. After releasing the H_2 pressure, the solution in the culture tube was transferred into two 5-mL glass vials in equal amounts using a 2.5 mL gastight syringe. Both of the solution aliquots were dried under vacuum. One was saved for TEM analysis; the residue in the other vial was dissolved in 2.5 mL of acetone added via a 5.0 mL gastight syringe. Cyclohexene (0.5 mL, 4.94 mmol) was then added to the solution using a 1.0 mL gastight syringe. The resultant solution was transferred via a disposable polyethylene pipet into a new 22×175 mm Pyrex culture tube containing a new $5/16 \times 5/8$ in. Teflon-coated stir bar. The culture tube was then sealed inside the F—P pressure bottle, brought outside of the drybox, placed inside a constant temperature circulating bath at 22.0 ± 0.1 °C, and attached via Swagelock TFE-sealed quick-connects to the hydrogenation line (which had already been evacuated for at least 30 min to remove any trace oxygen and water present, then refilled with purified H_2 at 40 ± 1 psig). The cyclohexene hydrogenation reaction was started exactly as in the Standard Conditions experiment and the catalytic activity of the redissolved iridium nanoclusters was determined by measuring the initial rate of the hydrogenation.

General Procedure for Catalyst Lifetime Experiments. Unless otherwise stated, all catalyst lifetime experiments were performed in the following manner and are based on our previously established reaction conditions.[26] In the nitrogen-filled drybox, 0.72 or 1.44 μmol of the catalyst (or precatalyst material) was weighed into a disposable glass vial and dissolved in 4.5 or 9.0 mL of acetone added with use of a 10 mL gastight syringe. The solution was mixed by agitation with a disposable polyethylene pipet. The resultant clear, homogeneous solution was transferred via a disposable polyethylene pipet into a new culture tube containing a new stir bar. Then, 4.5 or 9.0 mL (44 or 88 mmol, respectively) of cyclohexene was added to the solution with use of a 5.0 or 10.0 mL gastight syringe, respectively. The amount of cyclohexene corresponds to a maximum of 61 000 or 122 000 turnovers. The culture tube was then sealed inside the F—P pressure bottle, brought outside of the drybox, placed inside a constant temperature circulating bath at 22.0 ± 0.1 °C, and attached via Swagelock TFE-sealed quick-connects to the hydrogenation line (which had already been evacuated for at least 30 min to remove any trace oxygen and water present, then refilled with purified H_2 at 40 ± 1 psig). Stirring was started (at >600 rpm) and the F—P bottle was then purged 15 times with hydrogen (15 s per purge). A timer was started and the pressure in the F—P bottle was then set at a constant 40 ± 1 psig of H_2.

The reaction was monitored by periodically withdrawing aliquots of the reaction solution for ^{1}H NMR spectroscopy. Aliquots were

removed by stopping the timer, sealing the F—P bottle, disconnecting it from the hydrogenation line, transferring it into a drybox, releasing the H_2 pressure, and using a 9 in. glass Pasteur pipet inserted into the reaction solution in the culture tube to draw out ca. 0.05 mL aliquot. This aliquot was then added to 1 g of CD_2Cl_2 in an individual glass ampule and mixed with the Pasteur pipet. The solution in CD_2Cl_2 was then transferred into a NMR tube. The F—P bottle was then resealed, transferred back out of the drybox, reattached to the hydrogenation apparatus (which, in the meantime, has been evacuated for at least 30 min, then repressurized with H_2), and purged again 15 times with H_2 (15 s per purge) with vigorous stirring; the pressure was reestablished at a continuous 40 ± 1 psig of H_2. This procedure takes ca. 30 min and, therefore, does not introduce significant error in the stated, longer reaction times. The NMR tube containing the reaction aliquot in CD_2-Cl_2 was sealed and brought out of the drybox. The ^{1}H NMR spectrum of this solution gave directly the conversion of cyclohexene to cyclohexane.

Solution Molecular Weight Measurements. The details of the ultracentrifuge sedimentation—equilibrium molecular weight determinations of the form of the polyoxoanion present with, and without, added base are provided in the Supporting Information.

Supporting Information Available: A section titled A Closer Look at the Proper Use of the k_2/k_1 Ratio and Its Two Interesting Limits, Large vs Small k_2/k_1 Ratios; experimental details on Hydrogenations and Data Handling; full details for each experiment titled <u>Nanocluster formation and Cyclohexene Hydrogenation (Standard Conditions)</u>—Starting with $[Bu_4N]_5$-$Na_3[(1,5\text{-}COD)Ir \cdot P_2W_{15}Nb_3O_{62}]$ as Precatalyst; Starting with $[(1,5\text{-}COD)Ir(NCCH_3)_2]BF_4$ and $[Bu_4N]_9[P_2W_{15}Nb_3O_{62}]$; Starting with $[(1,5\text{-}COD)Ir(NCCH_3)_2]BF_4$ and $[Bu_4N]_3(C_6H_5O_7)$; Starting with $[(1,5\text{-}COD)Ir(NCCH_3)_2]BF_4$, $[Bu_4N]_3(C_6H_5O_7)$, and 1 equiv of Bu_4NOH; Starting with $[(1,5\text{-}COD)Ir(NCCH_3)_2]$-$BF_4$ and Poly(acrylic acid, tetrabutylammonium salt)—Starting with $[(1,5\text{-}COD)IrCl]_2$ without or with 1 equiv of Bu_4NOH; <u>Catalyst Lifetime Experiments</u>—Starting with $[Bu_4N]_5Na_3[(1,5\text{-}COD)Ir \cdot P_2W_{15}Nb_3O_{62}]$ as Precatalyst; Starting with $[(1,5\text{-}COD)Ir(NCCH_3)_2]BF_4$ and $[Bu_4N]_9[P_2W_{15}Nb_3O_{62}]$; Starting with $[Bu_4N]_5Na_3[(1,5\text{-}COD)Ir \cdot P_2W_{15}Nb_3O_{62}]$ and 1 equiv of Bu_4-NOH; Starting with $[Bu_4N]_5Na_3[(1,5\text{-}COD)Ir \cdot P_2W_{15}Nb_3O_{62}]$ and 1 equiv of $[Bu_4N]OH$ added after the first hydrogenation; Starting with $[(1,5\text{-}COD)Ir(NCCH_3)_2]BF_4$ and $[Bu_4N]_3(C_6H_5O_7)$; Starting with $[(1,5\text{-}COD)Ir(NCCH_3)_2]BF_4$, $[Bu_4N]_3(C_6H_5O_7)$, and 1 equiv of Bu_4NOH; <u>Figures:</u> Solution Molecular-Weight Measurements; Figure S-1, Ultracentrifugation sedimentation equilibrium solution MW plots for the heteropolyoxoanion present in the solution after cyclohexene hydrogenation of the precatalyst, $[Bu_4N]_5Na_3[(1,5\text{-}COD)Ir \cdot P_2W_{15}Nb_3O_{62}]$, with and without 1 equiv of added base; Figure S-2, Typical curve fit of the cyclohexene loss vs time in the hydrogenation of 1.6 M cyclohexene and concomitant formation of near-monodisperse 21 ± 3 Å $Ir(0)_{\sim 300}$ nanoclusters starting with $[Bu_4N]_9[P_2W_{15}$-$Nb_3O_{62}]$ and $[(1,5\text{-}COD)Ir(CH_3CN)_2]BF_4$; Figure S-3, Variations

in the total turnover number as a function of time in the cyclohexene hydrogenation starting with $[Bu_4N]_9[P_2W_{15}Nb_3O_{62}]$ and $[(1,5-COD)Ir(CH_3CN)_2]BF_4$; Figure S-4, Typical curve fit of the cyclohexene loss vs time in the hydrogenation of 1.6 M cyclohexene and concomitant formation of 23 ± 5 Å $Ir(0)_{\sim300}$ nanoclusters starting with 1.2 mM $[Bu_4N]_5Na_3[(1,5-COD)Ir \cdot P_2W_{15}Nb_3O_{62}]$ and 1 equiv of Bu_4NOH; Figure S-5, Variations in the total turnover number as a function of time in the cyclohexene hydrogenation starting with $[Bu_4N]_5Na_3[(1,5-COD)Ir \cdot P_2W_{15}Nb_3O_{62}]$ and 1 equiv of Bu_4NOH; Figure S-6, TEM image and associated particle size histogram of isolated, near monodisperse 23 ± 5 Å $Ir(0)_{\sim300}$ nanoclusters grown by hydrogen reduction of $[Bu_4N]_5Na_3[(1,5-COD)Ir \cdot P_2W_{15}Nb_3O_{62}]$ and Bu_4NOH; Figure S-7, Variations in the total turnover number as a function of time in the cyclohexene hydrogenation starting with $[Bu_4N]_3[C_6H_5O_7]$ and $[(1,5-COD)Ir(CH_3CN)_2]BF_4$; Figure S-8, The cyclohexene loss vs time plot in the hydrogenation of cyclohexene and concomitant formation of $Ir(0)$ nanoclusters starting with $[Bu_4N]_3[C_6H_5O_7]$, $[(1,5-COD)Ir(CH_3CN)_2]BF_4$, and 1 equiv of Bu_4NOH; Figure S-9, TEM image and associated particle size histogram of isolated 22 ± 5 Å $Ir(0)_{\sim300}$ nanoclusters grown by hydrogen reduction of $[Bu_4N]_3[C_6H_5O_7]$, $[(1,5-COD)Ir(CH_3CN)_2]BF_4$, and Bu_4NOH; Figure S-10, Curve fit of the cyclohexene loss vs time in the hydrogenation of cyclohexene starting with 6.0 mM poly(acrylic acid, tetrabutylammonium salt) and 1.2 mM $[(1,5-COD)Ir(CH_3CN)_2]BF_4$ (PDF). This material is available free of charge via the Internet at http://pubs.acs.org.

JA012749V